OXFORD

Intelligent Transportation Infrastructure, 2023, 1–20

https://doi.org/10.1093/iti/liad015

Review

Recent advances on research into high-speed railway noise†

Xiaozhen Sheng [1,2,*], Shumin Zhang[3], Xinbiao Xiao[4], Yuan He[5]

[1]School of Urban Railway Transportation, Shanghai University of Engineering Science, 333 Longteng Road, Songjiang, Shanghai 201620, China
[2]Shanghai Engineering Research Centre of Vibration and Noise Control Technologies for Rail Transit, 333 Longteng Road, Songjiang, Shanghai 201620, China
[3]School of Railway Rolling Stock, Shandong Polytechnic, 23000 Jingshidong Road, Jinan, Jinan 250104, China
[4]State Key Laboratory of Rail Transit Vehicle System, Southwest Jiaotong University, 111 First North Section, Second Ring Road, Chengdu, Chengdu 610031, China
[5]Institute of Sound and Vibration Research, University of Southampton, University Road, Southampton, Southampton SO17 1BJ, United Kingdom

*Corresponding author: School of Urban Railway Transportation, Shanghai University of Engineering Science, Shanghai 201620, China.
Email: shengxiaozhen@hotmail.com
†Special issue: Measuring, Monitoring, Modelling and Control of Railway Noise and Vibration

Abstract

Around 42,000 km high-speed railways are in operation in China with a maximum speed of 350 km/h. Trains which can run at 400 km/h are also under development. To control both train pass-by and train interior noise, huge resources have been put into research on high-speed railway noise, and the authors of this paper and their teams have been involved in several key projects. This paper is to summarise some of the advances achieved in these projects by covering the following topics: measurement results and characteristics of high-speed railway pass-by noise; analyses on source contribution to pass-by noise based on microphone array measurement; modelling of high-speed rolling, aerodynamic, and viaduct bridge noise; prediction of the vibro-acoustic behaviour of car-body with poro-elastic media; analyses of vibration transmission in the suspension/bogie system; statistical energy analysis-based prediction of train interior noise. Open problems and potential technologies for controlling high-speed railway noise are also discussed.

Keywords: high-speed railway, rolling noise, train pass-by noise, train interior noise, wheelset dynamics, track dynamics, wheel-rail interaction

1. Introduction

The main environmental impact of high-speed railway operation is noise pollution. As a train runs along a track at high-speed, both the train and track generate noise (railway noise). Main noise sources include rolling noise radiated by wheel/track vibrations (Thompson 2009), aerodynamic noise generated by, for example, bogies and pantographs (Thompson et al. 2015), and viaduct bridge noise due to vibration of the bridge structure (Li et al. 2018). The viaduct bridge noise is particularly a concern in China, since over 80 per cent of the high-speed railways are laid on viaduct bridges. There are other noise sources, such as those related to mechanical and electrical equipment in the driving and other auxiliary systems, but they are normally much less important when the train runs at high speeds. Sounds propagate from the noise sources to nearby environment, generating train pass-by noise which can largely degenerate the living quality of residents near the railway. Sounds also propagate from the sources to the interior space of the train, generating train interior noise, which normally has a negative effect on passengers' ride comfort.

China has seen a boom in high-speed railway since about 2008. By the end of 2022, around 42,000 km high-speed railways are in operation with a maximum speed of 350 km/h. Trains which can commercially run at 400 km/h are also under development. To control both pass-by and interior noise, huge resources have been put into research on high-speed railway noise, and the authors and their teams of this paper have been involved in several key projects. The purpose of this paper is to summarise some of the advances achieved in these projects. The following topics will be covered: measurement results and typical characteristics of high-speed train pass-by noise (Section 2); analyses on source contribution to train pass-by noise based on microphone array measurement (Section 3); modelling of high-speed rolling noise (Section 4), aerodynamic noise (Section 5), and viaduct bridge noise (Section 6); prediction of the vibro-acoustic behaviour of the car-body with poro-elastic media (Section 7); analyses of vibration transmission in the suspension/bogie system (Section 8); SEA-based prediction of train interior noise (Section 9). The paper is concluded in Section 10. A flowchart of the topics is shown in Fig. 1. It is seen that Sections 4–6 are about noise sources, while Sections 7 and 8 are about transfer paths of train interior noise. In most cases, train pass-by noise (Section 2) is determined mainly by the sources, while train interior noise (Section 9) depends not only on the sources, but also on the paths.

2. Characteristics of high-speed train pass-by noise

Pass-by noise of a typical 8-carrage Chinese high-speed train was measured for two track sections, a viaduct bridge section and an embankment section. The rail top of the viaduct bridge section

Received: July 22, 2023. **Revised:** August 17, 2023. **Accepted:** August 29, 2023

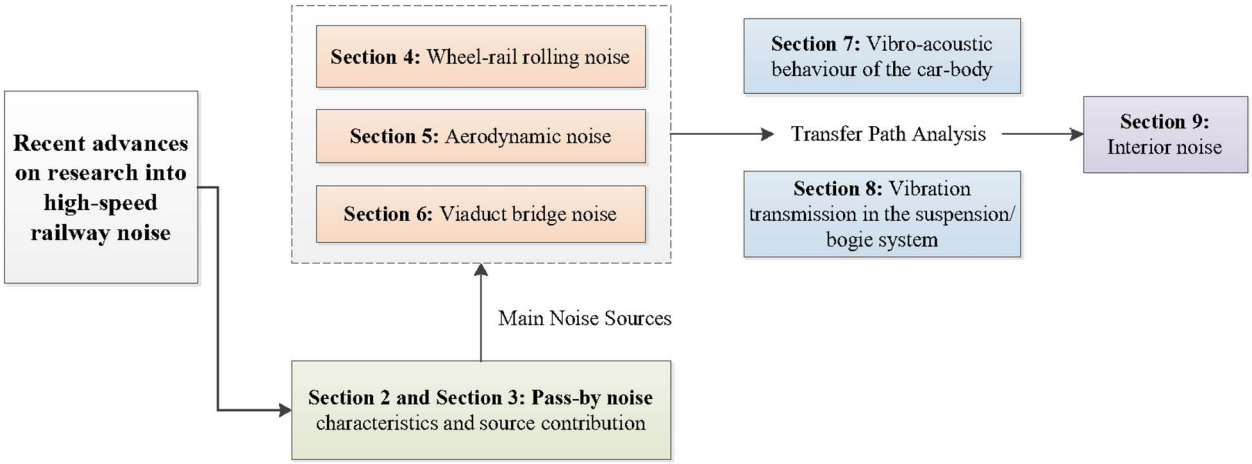

Figure 1. Topics covered in this paper.

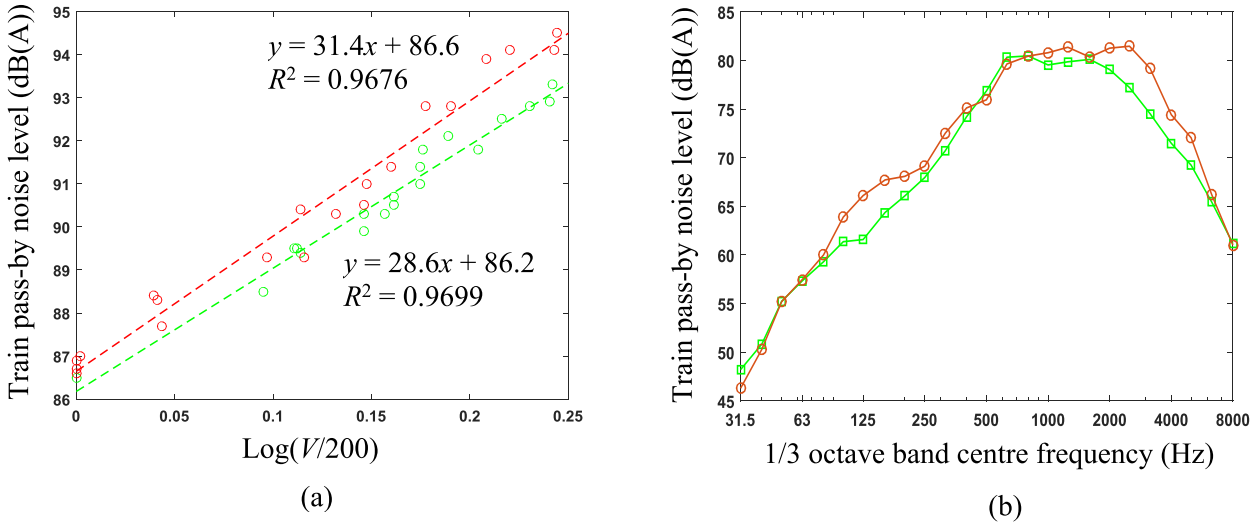

Figure 2. Measured train pass-by noise. (a) Overall levels; (b) 1/3 octave band spectra at 300 km/h. Red for the embankment section and green for the viaduct bridge section.

is about 10 m above the ground surface. Based on the measured pass-by noise data, Yang et al. (2019) presents an analysis on the characteristics of the pass-by noise and also discusses the difference in pass-by noise between the two track sections. For the measurement point 25 m away from the track central line and 3.5 m above the rail top, the pass-by noise levels are shown in Fig. 2a for a speed range of 200–350 km/h. It can be seen that the pass-by noise level near the embankment section is about 1–2 dB(A) higher than that near the viaduct section and the difference increases with train speed. This is mainly caused by the difference in the distance between the source/observer (i.e. the microphone) and the ground surface; the distance near the viaduct section is much greater than that near the embankment section, causing less sound reflection from the ground. Another feature of the pass-noise level is that the change of the noise level is related to train speed via approximately $30\log(V/V_0)$, where $V_0 = 200$ km/h. This indicates that, the overall level (20–5,000 Hz) in dB(A) of the pass-by noise is mainly contributed by wheel/rail rolling noise, even at 350 km/h.

The 1/3 octave band spectra of train pass-by noise at 300 km/h are shown in Fig. 2b. The measurement near the viaduct section is quieter than that near the embankment section for almost all the frequency bands. A common feature of the pass-by noise at these two measurement points is that the frequency range in which the noise levels are within 10 dB(A) of the maximum level is from 315 to 5,000 Hz.

Dependence of pass-by noise level on train speed can be worked out for each 1/3 octave band. The dependence, as in Fig. 2a, may be expressed as $L = a \times \log(V/200) + b$. When the train passes the measurement point near the viaduct section, the values of a are shown in Table 1 (train speed range 200–350 km/h). This table clearly indicates the dominating frequency range of the various sources (viaduct bridge noise, aero-dynamic noise, and rolling noise). By combining other evidences (see Sections 4.7 and 6), it may be concluded that at 350 km/h, below about 80 Hz, the pass-by noise is dominated by radiation from the bridge structure; between about 100 and 300 Hz, the pass-by noise is mainly aerodynamic, and above about 500 Hz, wheel/rail rolling noise is the main contributor. As pointed out above, the wheel/rail rolling noise dominates the overall pass-by noise level at that measurement point.

3. Analyses on source contribution to pass-by noise based on microphone array measurement

Both the track and train generate noise. Noise radiated from the track is purely vibro-acoustic, since the track only vibrates in air.

Table 1. Coefficients of dependence of pass-by noise level on train speed for each 1/3 octave band.

Frequency (Hz)	**25**	**31.5**	**40**	**50**	**63**	**80**	**100**	**125**
a	39.9	47.6	48.8	49.6	51.6	56.7	52.2	51.1
Freq. (Hz)	**160**	**200**	**250**	**315**	**400**	**500**	**630**	**800**
a	53.7	46.2	40.2	29.2	27.6	26.3	23.8	21.9
Freq. (Hz)	**1,000**	**1,250**	**1,600**	**2,000**	**2,500**	**3,150**	**4,000**	
a	26.3	32.7	30.4	25.6	29.4	34.3	36.0	

The wheelsets, however, not only vibrate, but also move in air, and therefore noise from the wheelsets is generated both vibro-acoustically and aerodynamically. Compared to the aerodynamic noise generated at high speed, noise radiated from the vibration of the bogie frames, train body, and pantographs is negligible. In other words, in terms of noise generation, these parts of the train can be regarded as moving rigid bodies without vibration. They generate noise mainly aerodynamically due to pressure pulsations on the body surfaces. There are turbulences around the train, and the turbulences are also noise sources (turbulence noise sources). However, it is well accepted that for pass-by noise, when trains run at 350 km/h or lower, the turbulence noise sources are not as important as body-surface pressure pulsations.

From the viewpoint of noise control, it is important to know the contribution of the various sources to pass-by noise so that the main contributors can be identified. Unfortunately, it is still difficult, although not impossible, to accurately quantify the sources (in terms of source strength, frequency content, and directionality) described above. For pass-by noise, however, the problem of noise source quantification may be approximately resolved by determining a set of equivalent point sources distributed in a vertical plane containing the side surface of the train. The projection of the train on the plane should be within the plane. The plane is termed the source plane of the train. The equivalent point sources in an area of the plane are attributed to the part of the train behind that area. In this way, the train can be divided into different areas (e.g. the pantograph area, the bogie aera, *etc.* see below for detail), and equivalent noise sources are determined for the areas. This may be achieved based on data measured using microphone array in the far field (Fig. 3a). According to the technique, the source plane is pre-divided into many small squares (they can be as small as 0.1 × 0.1 m, depending on the configuration of the microphone array), each square is regarded as an omnidirectional compact source, and all the compact sources are assumed to be incoherent. Under those conditions, the delay-and-sum and de-Doppler techniques are used to estimate sound powers for each square from the sound pressures measured by the microphone array. The sum of the sound powers of all the squares within an area (e.g. the bogie area shown in Fig. 3b) gives the sound power (called beam-forming sound power) of that area. In this way, noise sources on a moving train can be quantified and ranked, as done in Mellet et al. (2006) and He et al. (2014). The sound powers can also be used to develop models to quantify source contributions to pass-by noise, as done in Li et al. (2021a).

According to the model in Li et al. (2021a), the source plane is divided into a number of rectangular source areas. Ideally, source areas should be defined in such a way that, (1) they can fulfil the assumption of incoherent noise sources, meaning that each area must be sufficiently large; (2) they can give a good indication of the actual noise sources on the train; and (3) they can provide a direction for pass-by noise control. In Li et al. (2021a), seven types of source area are defined for each vehicle (see Fig. 3b):

(1) Bogie: there are sixteen bogies generating noise vibro-acoustically by wheel and rail vibrations, and aerodynamically by interaction between the moving bogies and air;
(2) Windshield: there are seven windshields generating noise aerodynamically;
(3) Cavity under windshield: there are seven such cavities generating noise vibro-acoustically by rail vibration, and aerodynamically by interaction between the train bottom and air;
(4) Car body: there are eight car bodies generating noise aerodynamically;
(5) Cavity under car: there are eight such cavities generating noise vibro-acoustically (by rail vibration) and aerodynamically;
(6) The first pantograph: generating noise aerodynamically;
(7) The second pantograph: generating noise aerodynamically.

Now at the centre of each source area is located an omnidirectional compact source having the same sound power as the beam-forming sound power of that area. To better consider the moving source effect, sound pressure spectrum due to a moving harmonic monopole, which is derived in Sheng et al. (2019), is utilised and the total sound pressure spectrum at a fixed point in the far field is synthesised to be an incoherent sum of those generated by the compact sources of the source areas. The contribution to pass-by noise of a type of area can be worked out by excluding contributions of all other types of area in the sum.

The pass-by noise predicted using the model is compared to measurement for the train runs along the viaduct track section at 350 km/h, as shown in Fig. 4. Good agreement is achieved, not only in sound pressure level time history, but also in frequency spectrum. This implies that data from microphone array measurement (including data processing) and the pass-by noise prediction model are workable. In terms of sound pressure level spectrum, the first three contributors are bogies, car bodies, and cavities under car. For frequencies higher than about 2,500 Hz, the car bodies, which mainly generate noise aerodynamically, are most important. For frequencies lower than 2,200 Hz, the bogies are most important. Regarding source contribution to pass-by noise time history, the bogies are the main contributors. Therefore, further pass-by noise control should be targeted at bogies.

Noise from the bogie area contains two parts, one being rolling noise and the other being aerodynamic noise. Pass-by noise models based on microphone array measurement, such as the one developed in Li et al. (2021a), cannot differentiate these two parts. More advanced models are desirable. Alternatively, the different noise sources and their contributions to pass-by noise may be predicted by developing appropriate predictive models.

Contributions to pass-by noise from the pantographs have been a concern for many. There are two pantographs. For the results in

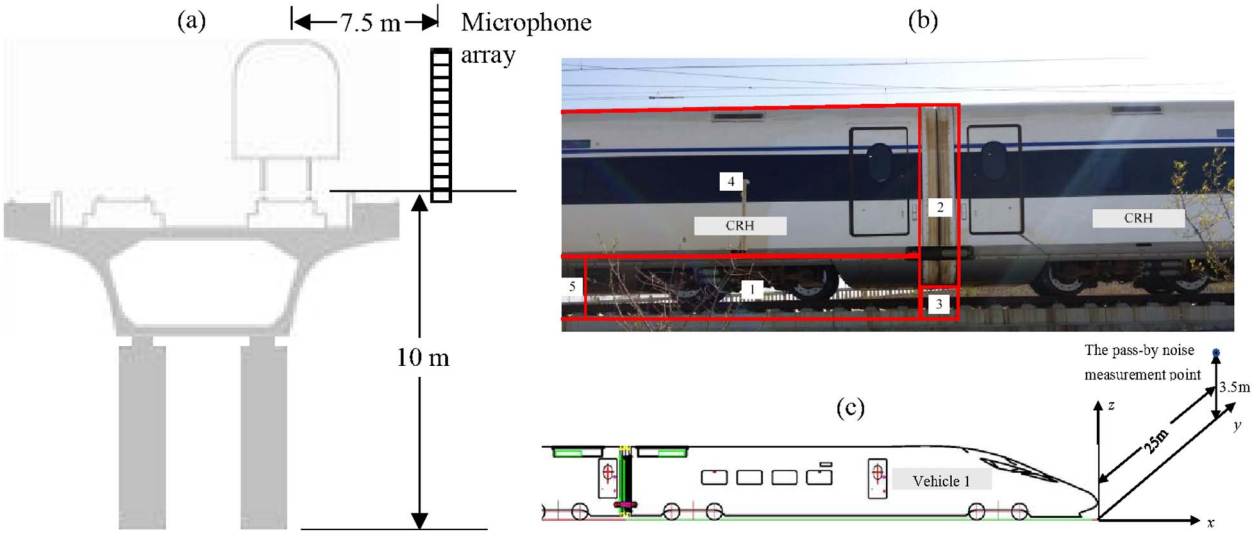

Figure 3. (a) Layout of microphone array measurement; (b) definition of source areas on the train; (c) the coordinate system and the pass-by noise measurement point.

Fig. 4, the first pantograph is the one on the third vehicle counted from the head car, and it is this pantograph which is used to collect electricity; the second pantograph which is on the sixth vehicle is at rest. Fig. 4a clearly shows the transient nature of the pass-by noise due to the pantographs. The instantly maximum level due to the first pantograph is similar to that due to bogies, and can be perceived by people near the track. Since the first pantograph is in use with a much shorter distance from the train head, contribution from this pantograph is much higher than that from the second pantograph which is at rest. However, in terms of contribution to overall pass-by noise level, the first pantograph only comes to the fourth, as shown in Fig. 4c.

4. Modelling of high-speed rolling noise

Modelling of wheel/rail rolling noise has been a research topic for over 40 years, mainly for ballasted track (Thompson 2009). Several rolling noise models have been developed with the TWINS model (Thompson et al. 1996a, 1996b) being most influential. In China, most of the high-speed railways are of slab track which have different acoustic characteristics from ballast tracks. It is also noticed that in the early developed models, factors which are important for high-speed trains, such as the rotation of the wheel and moving of the sound source, have not been adequately addressed. Efforts to improve these issues have been attempted in recent years by the authors of this paper and a description of the modelling approach is presented in Sheng et al. (2020). The approach is broken into six steps: (1) prediction of wheelset dynamics; (2) prediction of track dynamics; (3) prediction of wheel/rail interaction; (4) prediction of wheelset acoustics; (5) prediction of track acoustics; (6) prediction of wheel/rail rolling noise.

4.1. Prediction of wheelset dynamics

In this step, the vibration of a rotating wheelset (Fig. 5a) is calculated for a unit harmonic force applied at a wheel/rail contact point. A calculation method, in which all the effects of rotation are considered and use is made of the axisymmetric nature of the wheelset, is presented in Sheng et al. (n.d.). According to the method, the vibrational displacement of the wheelset is decomposed into two parts, one (termed rigid displacement) associated with the five rigid body motions of the wheelset and the other (termed elastic displacement) associated with the elastic deformation of the wheelset. The elastic displacement is described in a cylindrical coordinate system fixed to the wheelset, and is a 2π-periodic function of the circumferential coordinate. The partial differential equations of motion of the wheelsets are established by combining a 2D mesh (Fig. 5b) based-finite element scheme with the momentum law and the momentum torque law. By decomposing the elastic displacement into a number of components at particular circumferential orders, the partial differential equations become ordinary differential equations. It is shown that for steady-state solution, these ordinary differential equations can be solved algebraically. It is found that the displacement of the loading point (which is stationary in space) is also harmonic at the same frequency as the force. Thus, receptance can be readily defined and calculated for the wheelset at a wheel/rail contact point. This receptance can be used to deal with wheel/rail interaction, as explored in Sheng et al. (2016) and Zhang et al. (2020a). It is also found that, due to rotation, the load becomes a moving load when observed from the wheelset, and resonance no longer occurs at the modal frequency of the wheelset if the nodal diameter of mode is nonzero, but at two other frequencies, one lower and the other higher than the modal frequency. In other word, the peak at the modal frequency is split to two peaks by the rotation, as shown in Fig. 5c. It can be generally said that, the higher the rotation speed, or the larger the nodal diameter number of the mode, the wider is the split.

4.2. Prediction of track dynamics

This is to calculate track vibration due to a unit vertical harmonic wheel/rail force on each rail moving along the track. The methodology is developed in Sheng et al. (2017). A high-speed slab track is idealised to a periodic structure, with the period L being the length of a slab. In the direction of train motion, the slabs are numbered as $-\infty, \cdots, -1, 0, 1, \cdots\infty$. The origin of the x-coordinate is located at the junction between the -1th and 0th slabs. The harmonic load, $\mathbf{p}_0 e^{i\Omega t}$, is moving at speed c along the track. The response of the track at a given position x is temporally transient, thus having a finite frequency spectrum. It is shown in Sheng et al. (2017) that the spectrum at spectral frequency f is the sum of an infinite number of propagating waves. The wavenumber of the jth wave is β_j which is given by $\beta_j = \beta^* - 2\pi j/L$, where $\beta^* = (\Omega - 2\pi f)/c$ and $j = -\infty, \cdots, -1, 0, 1, \cdots, +\infty$. Formulae for

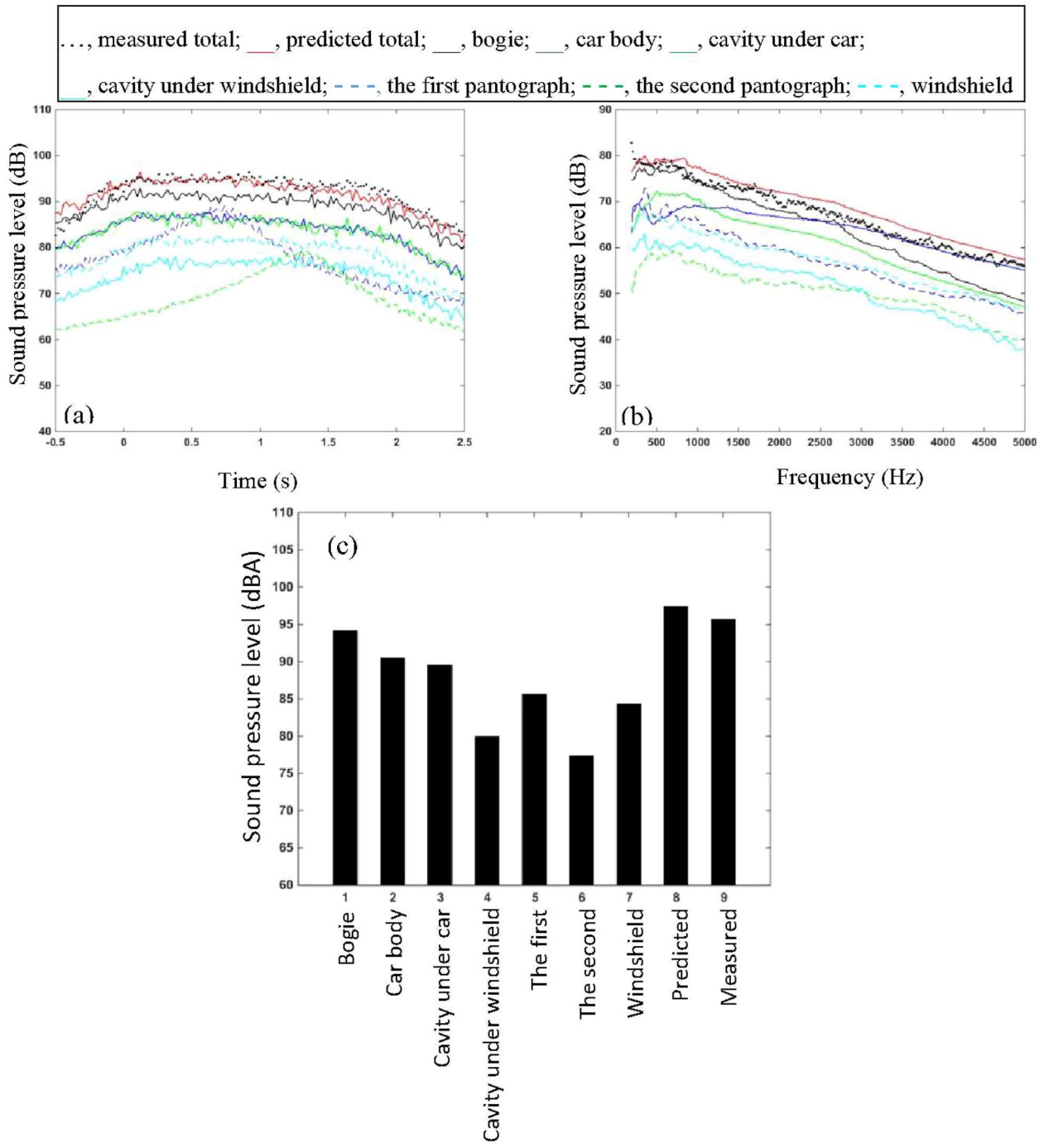

Figure 4. Source contributions to pass-by noise at 350 km/h with the first pantograph on the third vehicle counted from the head car being used to collect electricity, while the second pantograph on the sixth vehicle being at rest. (a) Time-history in dB; (b) spectrum in dB; (c) overall level in dB(A).

calculating the amplitude of the *j*th wave can be found in Sheng et al. (2017), which were derived following earlier work for ballast track (Sheng et al. 2005) and for the track with rail dampers (Sheng 2015).

4.3. Prediction of wheel/rail interaction

This is to calculate the wheel/rail forces generated from wheel/rail roughness as the wheelsets rotate and move along the track. The method developed in Sheng et al. (2007) is applied. According to the method, the combined wheel/rail roughness is assumed to be periodic in the track direction with the period being a multiple of the track period (i.e. NL, where N is an integer). Since the track is an infinitely long periodic structure with period L, and the receptance of a wheelset at the wheel/rail contact point can be defined (see Section 4.1) even though the wheelset is in rotation, the wheel/rail forces are also periodic in time with the period being NL/c, where c is the train speed. In other words, the wheel/rail forces contain components only at the fundamental frequency $c/(NL)$ and its multiples. As shown in Sheng et al. (2007), these frequency components of the wheel/rail forces can be worked out by solving a set of linear algebraic equations. A fine frequency resolution can be achieved by setting a large value for N.

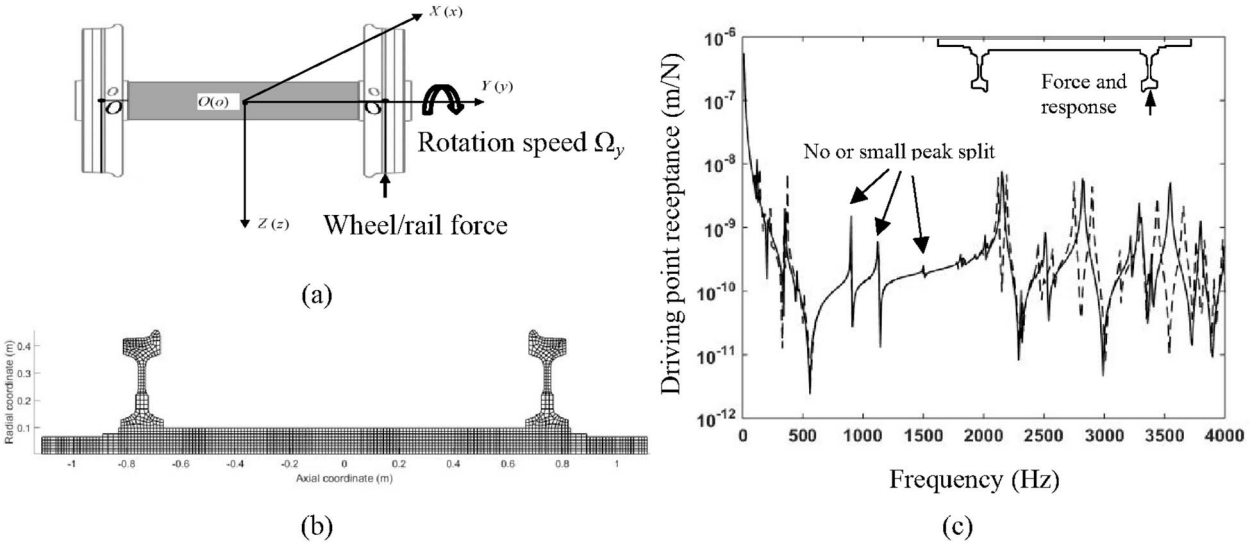

Figure 5. (a) The rotation wheelset; (b) the 2D FE mesh; (c) the vertical driving point receptance at the wheel/rail contact point (solid line for no rotation and dashed line for rotation at 300 km/h).

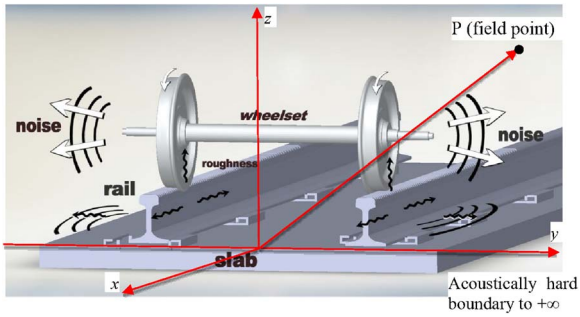

Figure 6. The acoustic domain.

4.4. Prediction of wheelset acoustics

This is to calculate the sound field generated by wheel vibration calculated in Section 4.1. For vibro-acoustics, an acoustic domain must be defined. In Sheng et al. (2020), the acoustic domain is approximated to be a half-space in which the slab is framed in an unbounded baffle, as shown in Fig. 6. For a stationary observer in space (P in the figure), the wheel is a moving noise source; the sound is therefore modified by Doppler Effect and aerodynamics. For a high-speed train, these effects can be significant and should be taken into account. However, a complete account of the effects is still difficult and simplifications have to be adopted. By neglecting the aerodynamic effects caused by wheel rotation and motion and assuming a sliding boundary condition on the surface of the wheel, it can be concluded that the particle velocity of the air in contact with the wheel surface is equal to the normal velocity of the wheel and is, therefore, also harmonic at the same frequency. By making use of sound spectra generated by moving harmonic compact sources (a monopole and a dipole), three-dimensional boundary integral equations are established in Sheng et al. (2019) for the prediction of sound radiated from a harmonically vibrating body moving uniformly in a free space. Currently, however, a numerical tool is still to be developed to solve this boundary integral equation. Thus, the following approximation is employed to evaluate sound radiation from the wheel.

First, the sound power of the wheel is calculated in the frame of reference moving with the train. In this frame of reference, apart from its rotation, the wheelset is stationary and vibrates harmonically, and its sound radiation can be predicted using the boundary element method. A 2.5D acoustic boundary element method (2.5D BEM), which only requires a 2D boundary mesh, can be derived for calculating sound power at each circumferential order, as described in Zhong et al. (2018). The total sound power is the sum of sound powers at individual circumferential orders. Then the wheel is simplified to be a point source moving uniformly in the track direction. This point source pulsates at the same frequency as the wheel and radiates the same sound power as predicted above. The sound pressure frequency spectrum of the moving point source is termed the *Wheel Sound Transfer Function*, denoted by $WSTF\left(f,\Omega,x_0\right)$, where, f is spectral frequency, Ω is the radian frequency of vibration, and x_0 is the x-coordinate of the wheel centre at $t=0$.

Recently, a new method is proposed in Theyssen et al. (2023) to calculate sound radiation from a moving wheel. Again, all the aerodynamic effects are excluded. There are four steps in the method: (1) sound pressures generated at a sufficiently large number of points on a reference sphere enclosing the wheel are calculated for each vibration mode; (2) based on the calculated sound pressures, sound pressure distribution on the sphere due to the vibration mode is expressed as a weighted sum of a set of spherical harmonics so that the modal acoustic impulse function of the mode can be produced for the wheel at different longitudinal positions; (3) the modal acoustic impulse function is then used to calculate pass-by noise (sound pressure time-history) of the mode through a convolute integral; (4) pass-by noises due to individual modes are added together to give the pass-by noise of the wheel. From these steps, it can be felt that the computational efficiency might be an issue.

4.5. Prediction of track acoustics

This step is to calculate sound pressure generated by the track due to the vibration predicted in Section 4.2. In the calculation, connections (fasteners) between the rails and the slab are removed, leaving a uniform gap between the rail and the slab. The sound pressure is the sum of that generated from slab vibration and that from rail vibration. These two sound pressure components are computed separately. For sound generated just from slab

vibration, the two rails are removed. The sound pressure at a given location in the acoustic domain may be produced for a slab vibrational velocity wave defined by $\Phi_j(y)e^{i\beta x}e^{i2\pi ft}$ for a range of spectral frequencies (f), wavenumbers (β), and lateral shape function $\Phi_j(y)$. Shape functions are introduced to describe variation of slab vibration in the lateral direction. This will generate a number of so-called *Slab Sound Transfer Functions* (SSTFs). The SSTF for the jth shape function $\Phi_j(y)$ is denoted by $SSTF_j(f,\beta)$. Since the slab is equivalent to an infinitely long baffled plate, its sound radiation may be calculated using an integral equation which is derived by performing Fourier transform on the classic Rayleigh integral equation with respect to the longitudinal (i.e. x) coordinate.

For sound radiation from the vibration of a rail, the slab is assumed to be acoustically hard behaving as a pure reflector. As for the slab, a number of so-called *Rail Sound Transfer Functions* (RSTFs) may be produced using the 2.5D BEM for a rail structural wave for a range of spectral frequencies (f) and wavenumbers (β). Another set of shape functions are introduced to express vibration variation along the cross-sectional boundary of the rail. The RSTF is denoted by $RSTF_k(f,\beta)$ for the kth shape function. The mirror principle is applied to avoid meshing the infinitely wide acoustically hard boundaries.

4.6. Prediction of wheel/rail rolling noise

This is the last step. It is to calculate the sound pressure spectrum of the rolling noise by adding up contributions from all the wheels, the rail, and the slab due to all the frequency components in all the wheel/rail forces. As shown above, the wheel/rail force contains components at fundamental frequency $f_0 = c/(NL)$ (L is the slab length, NL is the period of the wheel/rail roughness). The kth harmonic component at the lth wheel is denoted by $\tilde{P}_{lk}e^{ikf_0t}$. The initial x-coordinate of the lth wheelset is denoted by x_{l0}. The sound pressure spectrum is given by

$$|\hat{p}(f)|^2 = \sum_k \sum_l \left(\left| \hat{p}_{Wlk}(f, x_{l0}) \right|^2 + \left| \hat{p}_{Rlk}(f, x_{l0}) + \hat{p}_{Slk}\left(f, x_{l0}\right) \right|^2 \right) \quad (1)$$

where $\hat{p}_{Wlk}(f, x_{l0})$ denotes the sound pressure spectrum generated by the lth wheel subject to the kth harmonic component in the lth wheel/rail force. Equation (1) shows that, at a given frequency (e.g. the kth) in a wheel/rail force (e.g. the lth), the sound pressure spectra generated by the rail and slab are added together coherently, and then the resultant is added with that from the wheel incoherently. It is also seen from Equation (1) that contributions from the different frequency components of the different wheel/rail forces are added incoherently.

4.7. Results

Rolling noise is predicted for the site described in Section 2, and is shown and compared with measured pass-by noise in Fig. 7. It can be seen from Fig. 7a that the predicted overall rolling noise is close to the measured overall pass-by noise, indicating the dominance of the rolling noise over other noise sources. At 350 km/h, rolling noise dominates the pass-by noise for frequencies higher than about 500 Hz, as shown in Fig. 7b. For frequencies lower than 500 Hz, the predicted rolling noise is much lower than the measured pass-by noise, indicating that other noise sources dominate the pass-by noise at these frequencies. At this observation point, it is predicted that, for 500–2,000 Hz, rolling noise is mainly due to rail radiation but higher than 2,500 Hz,rolling noise is mainly from the wheels. However, in terms of overall level, it is predicted that the rail contributes more than the wheels.

The model described in Sheng et al. (2020) is still being improved. Simplifications which have been taken in the model, for various reasons, brings certain uncertainty into the predicted results. An investigation into the effects of modelling assumptions on sound power radiated from a high-speed train wheelset is presented in Cheng et al. (2021). As stated above, the periodic nature of the gap between the rail and slab is replaced with a uniform gap. The effect of doing so is still under investigation. So far, all the rolling noise models, including the one in Sheng et al. (2020), have been developed by assuming that the wheel and rail are in still air without any airflow. This is not true for high-speed trains. The effect of airflow generated by a train on the sound propagation from the wheel and rail is unclear.

Rolling noise may be controlled by using tuned mass rail dampers and tuned mass wheel dampers. A wheelset with tuned mass dampers is no longer an axisymmetric structure, but a cyclically periodic one. This will further complicate the analysis of wheelset dynamics and acoustics.

5. Modelling of high-speed aerodynamic noise

Train aerodynamic noise becomes more and more concerned as train speed gets higher and higher. Research before 2015 in the prediction and control of aerodynamic noise from high-speed trains is reviewed in Thompson et al. (2015). The main aerodynamic noise sources of a high-speed train include the pantographs, the bogies, the train nose, the gaps between coaches (the gaps can be eliminated by using fully enclosing windshields), and the wake region. Of the various noise sources, the bogies and pantographs are most important. The pantographs are located at the top of the train roof and therefore, it is hardly affected by noise barriers installed along railways. The bogies, which usually have very complex geometry, are under the train body. The number of bogies is much greater than that of pantographs; thus, noise contribution to pass-by noise from the bogies is much greater than that from the pantographs, as shown in Fig. 4c.

5.1. Wind tunnel measurement

The generation of aerodynamic noise of a high-speed train is related to the turbulent flow field around the trains. To study the characteristics of the noise, experiment is a direct and effective option. Experimental tests are carried out most often with wind tunnels. At present, results from wind tunnel tests are still the most reliable. Detailed and comprehensive wind tunnel tests can help locate aerodynamic noise sources and understand the mechanism of aerodynamic noise generation, providing targeted guidance for noise reduction design. On the other hand, in the development of high-speed trains, the verification of the noise reduction effect brought about by design changes is usually verified through wind tunnel tests, especially when a prototype vehicle has not been produced. Wind tunnel test is also the best way to verify the accuracy of the numerical simulations. More importantly, by detailed benchmarking with wind tunnel test results, best practice criteria can be established for a certain type of numerical simulation (such as aerodynamic noise simulation of high-speed train pantographs and bogies), including grid strategy, time step size, turbulence model, etc.

For high-speed trains, due to size limitation of the wind tunnel itself, wind tunnel tests can only be conducted on downscaled models. To ensure the similarity of the flow field between the downscaled model and the full-scale model, certain conditions

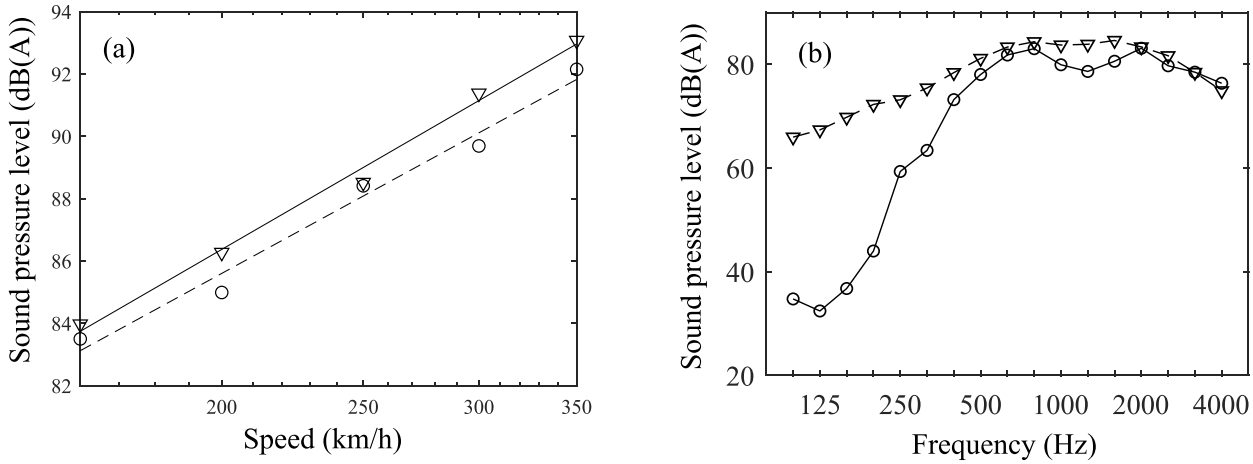

Figure 7. Measured train pass-by noise (triangle) and predicted rolling noise (circle) for the measurement point 25 m away from the track central line and 3.5 m above the rail top at the site described in Section 2. (a) Overall level for a speed range between 160 and 350 km/h; (b) 1/3 octave band spectrum at 350 km/h.

need to be met, such as a sufficiently high Reynolds number. Some acoustic similarity laws have also been developed for the conversion of acoustic results between scaled models and full-scale models. From the results presented in some literature, the effectiveness of the noise reduction measures determined based on the downscaled model has also been verified in *in situ* tests. This to some extent indicates that downscaled modelling can be used for noise reduction research of high-speed trains.

As shown in Fig. 8, Zhao et al. (2020) use the particle image velocimetry to test a 1:40 scaled train model consisting of a leading carriage and a tailing carriage with a simplified pantograph and a groove on the roof. The main purpose of the experiment is to generate data to validate the corresponding numerical model, so that the numerical methodology can be applied with confidence to a 1:3 scaled high-speed trains with three carriages. The test flow speed is 27.8 m/s, flowing from the left to the right; the mean vorticity field on the symmetry plane as well as the pressure fluctuations at point1 and point2 shown in Fig. 8 are obtained. The result of the vorticity field shows that the greatest vorticity value appears in the groove. In addition, it shows that the vorticity values significantly decline after passing through the inter-coach gap. This is consistent with the conclusion that the pressure fluctuation intensity of point1 is greater than that of point2. It is believed that the inter-coach gap attenuates the flow fluctuations from upstream. This experiment reveals the flow characteristics after the pantograph and around the gap. In the corresponding numerical simulations, the results show that the solid surface of the pantograph, the groove, and the gap has strong noise sources. Therefore, it is reasonable to conclude that the origin of the noise generation is the highly turbulent flow at the car roof.

As seen in Fig. 9, Li et al. (2022) conducted an experimental measurement of the aerodynamic noise produced by a 1:3 scaled high-speed train model in Shanghai Automotive Wind Tunnel Centre at Tongji University. To simulate the flow around the leading bogie, the train nose and cowcatcher are retained, while the rear carriages are instead by a train tail. The inflow speed is around 69.5 m/s (250 km/h). The spectra of the far-field noise are broadband and humps are found near 400 Hz (this frequency will decrease if the model is full-scaled). Furthermore, sound source map is also obtained using a microphone array. It is shown that the bogie region emits the highest noise than other region, such as the train nose and the bottom of the cowcatcher.

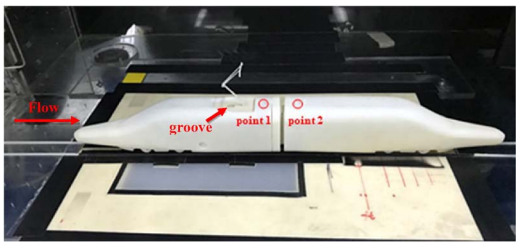

Figure 8. The test model in the study of Zhao et al. (2020). Wind is from the left to the right.

Figure 9. Train nose car model of the test conducted by Li et al. (2022).

This conclusion is in good agreement with the measurements carried out by Lauterbach et al. (2012) and Mellet et al. (2006).

Although experiments have been carried out in wind tunnels, there are several issues that need to be paid attention. In the test of pantograph noise, the effects of some factors have not been considered, such as the turbulence of the flow and the cross wind. These factors will affect the vortex shedding on the components of the pantograph and the noise is thereby affected. Moreover, in the test of bogie noise, the effect of the ground has not been sufficiently considered because it is difficult to simulate the moving ground in the wind tunnel. However, the moving ground has effect on the bottom flow field because of the interaction between the shear layer at the bogie bottom and the boundary layer on the ground (Zhu et al. 2017). This interaction will enhance the pressure fluctuations on the surface of the bogie and its cavity and thereby the noise source intensity increases. To solve these issues, field test is an alternative. However, there are some difficulties in the field test. These difficulties contain the control

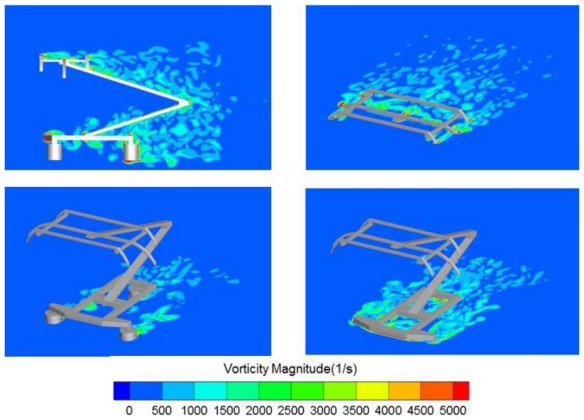

Figure 10. The vorticity field around a pantograph (Shi 2020).

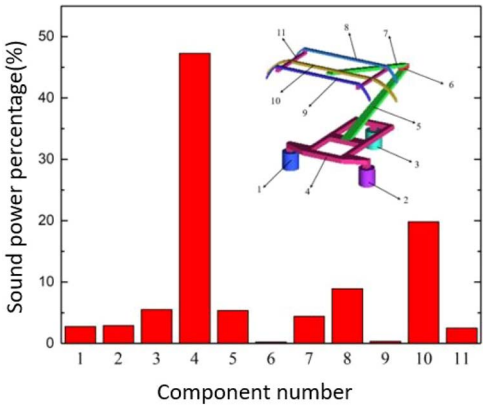

Figure 11. Proportion of radiated sound power of pantograph components (Shi 2020).

of the local flow condition and the separation of the aerodynamic noise and rolling noise in the noise measurements.

5.2. Numerical study on aeroacoustics of pantograph

Apart from the experimental methods, numerical simulation is another option that can facilitate the understanding of the noise generation mechanisms of high-speed trains. Compared with the experimental methods, the numerical simulation has merits of low cost, easy control of flow conditions, and ability of providing flow properties at any position. Nevertheless, due to the physical scale and the complex geometry of trains, there are also several difficulties in the numerical simulation of the train noise, e.g. the mesh generation, the high computational cost, and the calculation of the reflection and scattering of sound.

A pantograph consists of cylinders whose cross-section is circular or approximately square. Thus, its geometry is not too complex. To discretise a pantograph model, the trimmed mesh generated by commercial software, such as star CCM+, can be adopted. In a simulation, the first boundary layer grid should be adjusted to guarantee that the $y+$ is smaller than 1. However, this usually makes the grid number huge. Fig. 10 shows the vorticity field around the pantograph (Shi 2020). It can be seen that the vorticity value is high behind the pantograph components. For the upstream components, there is vortex shedding, which generates high pressure fluctuation on the solid surface. For the components downstream, they are impinged by the wake flow generated by the upstream components. This impingement enhances the pressure fluctuations on the solid surface and the noise source intensity is stronger than that of the upstream components. Figure 11 illustrates the sound power contribution from the different components of the pantograph. It can be seen that the sound power of the downstream horn is greater than that of the upstream one. In the lower part, the frame has the greatest contribution of sound power because it has great surface area. In the upper part, the middle horn contributes the most because it is the longest among the three horns.

High-speed railways in China have been extended to the area of high latitude where the environment temperature is very low. The low temperature has effect on air density and viscosity, which has effect on the aerodynamic forces and noise. Numerical simulations of the performance of a high-speed train in low temperature area are carried out in Shi (2020). The results show that, at 400 km/h, when the air temperature drops to −50 °C, the averaged sound pressure level of the pantograph is 3.5 dB greater than that at 15 °C at measurement points on a horizontal semi-circle with a distance of 7.5 m from the pantograph. In addition, the lift fluctuation of the upper part of the pantograph also becomes stronger. The reason of these changes is believed to be that the increased air density makes the pressure fluctuations stronger. However, the spectrum characteristics of aerodynamic noise at different temperatures are similar.

5.3. Numerical study on aeroacoustics of bogie

Due to the complexity of the geometry of train bogie, it is extremely hard to carry out numerical simulations with a grid with good quality and fine enough density. As seen in Fig. 12, He (2023) explored a hybrid grid which consists of a structured grid near the solid surface and polyhedral grid at the rest of the volume. This grid can guarantee a good grid quality in the boundary layer and a flexibility at the region away from the solid surface. It is then adopted to discretise a model of a bogie from the leading car of a high-speed train. It is seen that the head vehicle in the figure is assumed to be a locomotive although the Chinese head vehicle is usually a trailer. The Delayed Detached Eddy Simulation is used to investigate the flow and obtain the noise source information to feed into the Ffowcs Williams–Hawkings acoustic analogy for far-field noise prediction. Figure 13a shows the noise source distribution on the model surface. The noise source is visualised by the root-mean-square value of the pressure change rate (dp/dt). The regions with strong pressure fluctuation intensity are the bottoms of the cowcatcher and the bogie, the side components of the bogie, and the rear wall of the bogie cavity. Figure 13b shows the 1/3 octave noise spectra of the model at a side receiver 20 m away (full scale) from the centre of the bogie. The noise generated by the ground was not considered. The spectra are broadband with no tonal peaks. The noise spectrum of the car body is greater than that of the bogie at all frequencies. In addition, it is noted that the spectra have a broad peak around 100 Hz (full scale). Similar conclusions can be found in the experiments of (Latorre Iglesias et al. 2017).

Based on the analysis of the flow field and pressure fluctuation distribution of the simulated cases, a noise control technique based on a dual staggered jet is developed to reduce the noise level of the leading car. The wake at the bottom and the detached shear layer at the two sides of the cavity is pushed away by the jets, which reduces the pressure fluctuations on the bogie and the cavity. A reduction of 2 dB for the sound pressure levels and 3.5 dB for the sound power levels is obtained.

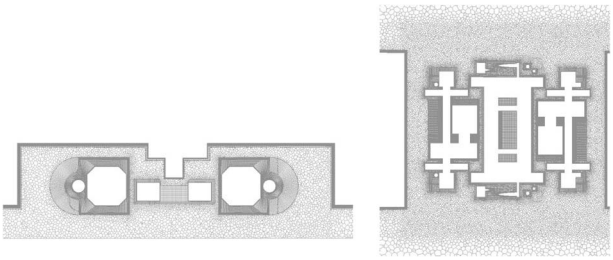

Figure 12. The hybrid grid used in the study of He (2023).

Although many experimental and numerical researches have been carried out, there are still several challenges in the study of the aerodynamic noise of high-speed trains. In both experimental and numerical studies, the physical model and the flow speed are scaled down to reduce the research cost. Therefore, the first one is the determination of the aero-acoustic scaling laws. The second challenge is how to simulate the ground condition of the test model. The flow at the bottom of the bogie is very chaotic; it is a very important source of noise generation. However, experiments in wind tunnel are difficult to simulate the motion of the ground, especially for the ballast track on the ground. The third challenge is the calculation of the sound propagation at the bogie region. In the current numerical simulations, the sound reflection and scattering are not considered because the geometry of the bogie is very complex which makes the computational cost extremely high.

6. Modelling of high-speed viaduct bridge noise

Noise radiated from viaduct bridges has been a concern in China, since over 80 per cent of the high-speed railways are laid on viaduct bridges. Questions are asked about the major frequency range, contribution to the overall pass-by noise, attenuation law, etc. It is evident that measurement only cannot answer all these questions, and therefore development of prediction models becomes an important research topic for many researchers (Zhang et al. 2013; Li et al. 2014). Due to the high-speed and low frequency nature of high-speed viaduct bridge noise, the motion of the entire train and many spans of bridge must be taken into account. This is achieved in He et al. (2021).

The approach taken in He et al. (2021) is similar to that used for modelling rolling noise (see Section 4). The track/bridge structure is idealised as an infinitely long periodic structure with the period being the length of one bridge (Fig. 14a). The response of the rail due to a moving harmonic force can be calculated using the method similar to that in Section 4.2. To calculate the receptances of fasteners seen by the rail, the finite element method has to be used since we are now including a bridge span. The train is modelled as a linear multi-rigid body system for which receptance can be worked out for the train at each wheelset. Wheel/rail roughness is also assumed to be periodic with the period being a multiple of the bridge length. With the receptance of the train at the wheelsets and the rail response to a moving harmonic load, wheel/rail forces can be worked out, as in Section 4.3. Since the geometry of the radiating surface is the same for all the bridges, the radiating surfaces form an acoustic boundary which is uniform in the track direction and sound radiation from all the bridges can, therefore, be predicted using the 2.5D acoustic boundary element method which only requires a 2D mesh along the boundary of the cross-section (Fig. 14b). As shown here, the track slab is taken as a part of the bridge (since generally it is firmly connected with the bridge deck), and the predicted bridge noise includes that radiated from the track slab.

Bridge noise is predicted for the site described in Section 2, and is shown and compared with measured pass-by noise in Fig. 15. It can be seen from Fig. 15a that bridge noise dominates the pass-by noise only for low frequencies up to about 80 Hz. Distribution of bridge noise in the mid-span vertical plane is shown in Fig. 15b, and the nosiest area is to the northeast of the wing. A parameter study is performed using the model for bridge noise. Studied parameters include train speed, fastener stiffness, under-track slab stiffness, the stiffness of the bridge support on the abutment. It is found that a relationship $L = a\log(V/200) + b$ may be written between bridge noise level (L, dB) and train speed (V), with a being about 35 for the site (He et al. 2021); a lower fastener stiffness or a lower bridge support stiffness result in a lower bridge noise level; however, a reduction in under-track slab stiffness increases radiation from the slab, resulting in a higher bridge noise.

The principle of acoustic short-circuit may be used to reduce bridge noise, as shown in Fig. 16a where sixteens holes of 0.75 m diameter are made on the two wings of each bridge to make acoustic short-circuited. The effect is shown in Fig. 16b, and the overall reduction is about 3 dB.

7. Prediction and control of the vibro-acoustic behaviour of car-body with poro-elastic media

For large countries or continents, passengers may travel on high-speed trains up to 10 h. For those passengers, low interior noise is much desired. Train interior noise has two major parts from two transfer paths. The first one is airborne: this part is radiated by the part of car body vibration which is excited by noise (such as rolling noise and aerodynamic noise) outside the train. To control this part of interior noise, the sound transmission loss (STL) of the car body should be sufficiently high by proper vibro-acoustic design. The second one is structure-borne: this part is radiated by the other part of car body vibration which is excited by the dynamic forces applied by the elements in the secondary suspension to the car body. These forces depend not only on the intensity of wheel/rail interaction, but also on the dynamic property of the bogie/suspension system.

The airborne interior noise of a high-speed train may be controlled at source by reducing rolling noise, aerodynamic noise, and/or wheelset vibration. However, it can be more effectively controlled by making the car body less efficient in sound transmission while keeping it sufficiently light. Since the car body is too complicated and large to study its vibro-acoustics in a detailed manner, it is common to cut a part (e.g. the floor) from the car body to study the vibro-acoustic behaviour of that part. Figure 17 shows the floor structure (a composite panel) of a typical high-speed train. A wooden floor is supported by wooden beams resting on an aluminium extrusion. Layers of poro-elastic media are filled between the wooden floor and the aluminium extrusion for both sound and heat insulation. A model to predict the STL of the composite panel is required so that parameters of the composite panel can be designed to achieve the required STL. The complexity of the structure and the presence of the poro-material make the modelling a great challenging task. Simplification should be made whereover possible.

Since the longitudinal dimension of the panel is much larger than other two dimensions and its cross-section geometry and

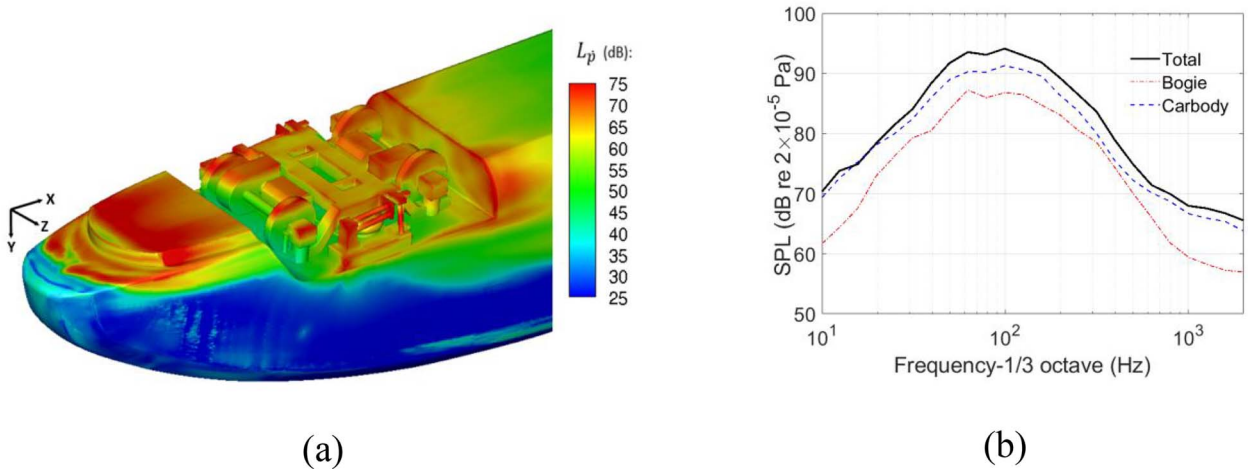

Figure 13. Aerodynamic noise from the leading bogie (He 2023). (a) The surface contours of the pressure fluctuation intensity; (b) one-third octave noise spectra at full scale for a speed of 400 km/h and distance 20 m.

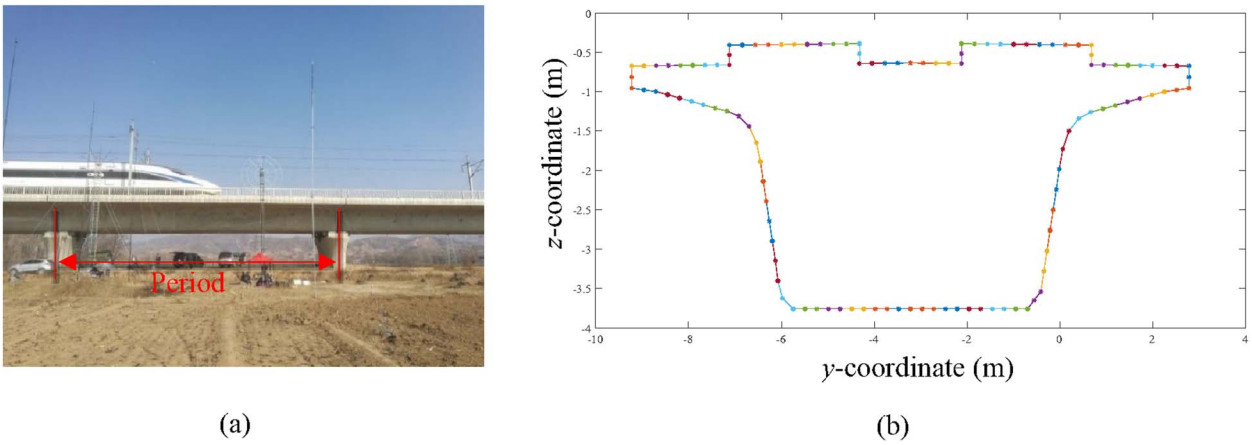

Figure 14. Prediction of bridge noise. (a) The viaduct bridge as an infinitely long periodic structure; (b) the 2D boundary mesh.

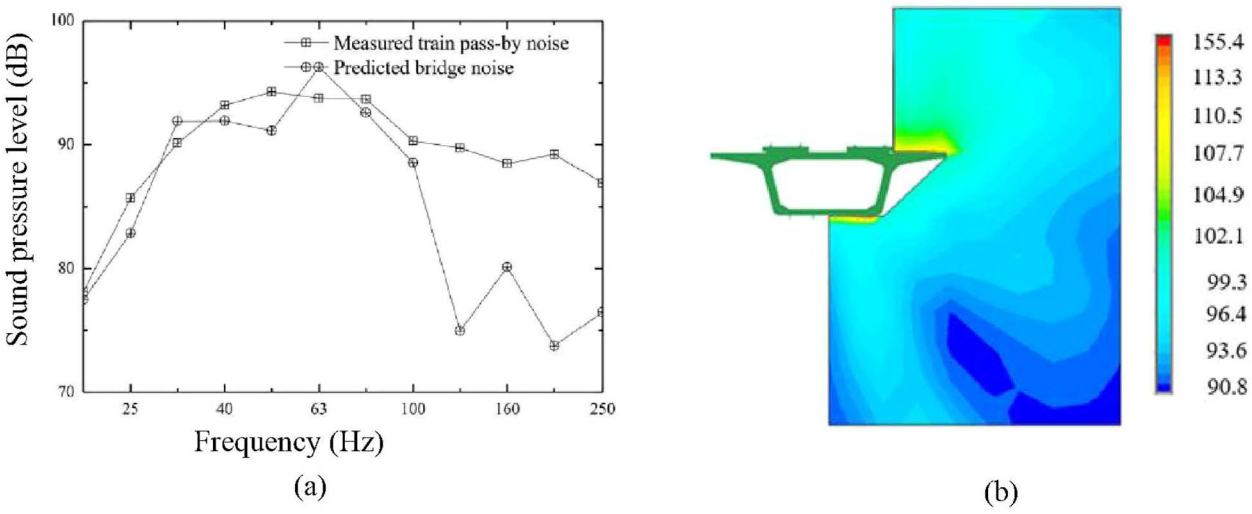

Figure 15. Predicted bridge noise and measured pass-by noise for the measurement point 25 m away from the track central line and 3.5 m above the rail top at the site described in Section 2. (a) The measured pass-by noise and predicted bridge noise; (b) distribution in the mid-span vertical plane of bridge noise.

material properties are almost uniform in the longitudinal direction, the structure may be idealised to be infinitely long and uniform in the longitudinal direction, making it a two-and-half dimensional (2.5D) structure. The panel is further assumed to be baffled. Based on such idealisation, a 2.5D vibro-acoustic model is developed in Deng et al. (2021). In this model, the solid structure is treated as elasticity and modelled using the 2.5D finite element method. For the porous material, of which the elasticity of the

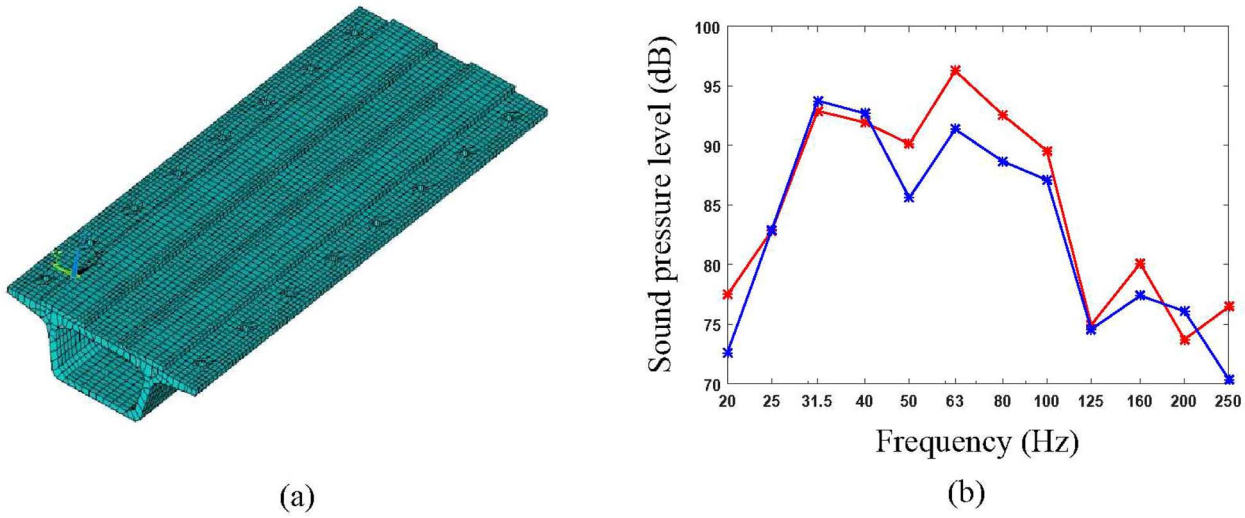

Figure 16. Bridge noise reduction using acoustic short-circuit. (a) Sixteen holes of 0.75 m diameter on the wings; (b) sound pressure spectrum without (in red) and with (in blue) the holes.

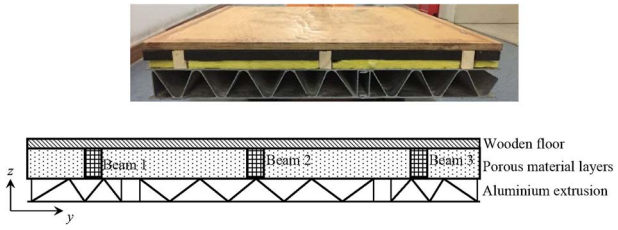

Figure 17. The cross-section of the floor structure of a typical high-speed train.

frame or skeleton must be considered, the Biot's poro-elastic theory (Biot 1956a, 1956b) is employed, and the corresponding 2.5D finite element method is developed in which the displacement of the skeleton and the in-pore pressure of the fluid are used to describe the state of the porous material. Air in the voids of the aluminium can be modelled using the 2.5D finite element method for fluid but it is found that the air has negligible effect on the vibro-acoustics of the composite panel (Zhang et al. 2018) and therefore for simplicity, it is excluded in the model of Deng et al. (2021). Since the composite panel is flat and thin compared to the acoustic wavelengths considered, the sound field either side of the panel can be modelled using the Rayleigh integral in the wavenumber domain.

For a solid in the panel, there are only four parameters, i.e. density, Young's modulus, Poisson's ratio, and damping loss factor. For a porous material though, the material parameters are much more, including tortuosity, porosity, flow resistivity, viscous and thermal characteristic lengths of the porous material, and the density, Young's modulus, Poisson's ratio, and loss factor of the frame in vacuum.

The model has been used to study STL of various composite panels. The panels are infinitely long and uniform in the longitudinal direction and are baffled. On the two sides in contact with the baffle, the wooden floor, aluminium extrusion, and skeleton of the porous material are simply supported, while air particle velocity is set to zero. As shown in Fig. 18a, an incident sound wave propagates toward the panel at angles defined by φ, ψ, and θ in Acoustic domain 1, and the sound wave transmitted by the panel into Acoustic domain 2 is predicted, so that STL of the panel can be estimated for each and every set of incidence angles. These STLs are then used to calculate the diffuse STL for the composite panel (Fig. 18b). It can be seen from Fig. 18b that the STL at low frequencies (lower than the first dip frequency) is determined by the stiffness of the panel, slightly affected by the porous material (they change the weight of the panel to some extent). The dip is caused by the resonance of the panel or the resonance of the wooden floor on the porous material layer. Figure 18b demonstrates the great influence of porous layer configuration on the STL at higher frequencies if the wooden beams were not present (see Fig. 17). However, with the wooden beams, the STL (not shown here but, see Deng et al. [2021]) is largely reduced and the role of the porous layers become much less significant. This is because vibration can be efficiently transmitted by the beams and the porous material behaves mainly as added mass. It is further found that STL can be significantly increased by applying a porous layer on the outer surface of the aluminium extrusion. Of course, there are practical difficulties which need to be tackled when applying a porous layer on the outer surface of the car body of a high-speed train.

8. Analyses of vibration transmission in the suspension/bogie system

To control train interior noise effectively, it is critical to know which part, the airborne part or the structure-borne part, is dominant in a frequency band. Unfortunately, so far there is still no effective technique that can be used to fully answer the question. Nevertheless, serval techniques have been attempted for interior noise path analysis. For example, the operational transfer path analysis (OTPA) technique has been tried to identify transfer paths for interior noise (Ström 2014; Noh 2017; Li et al. 2021b), but the results are to be verified by other methods since 'cross-talks' of the paths are unavoidable in a high-speed train.

The structure-borne part of interior noise may be predicted if the forces applied to the car body are known. Direct measurement of the forces under operational condition is difficult and even impossible, making the indirect determination of the forces an important research topic. The forces may be determined from structure vibration by solving an inverse problem. There are two

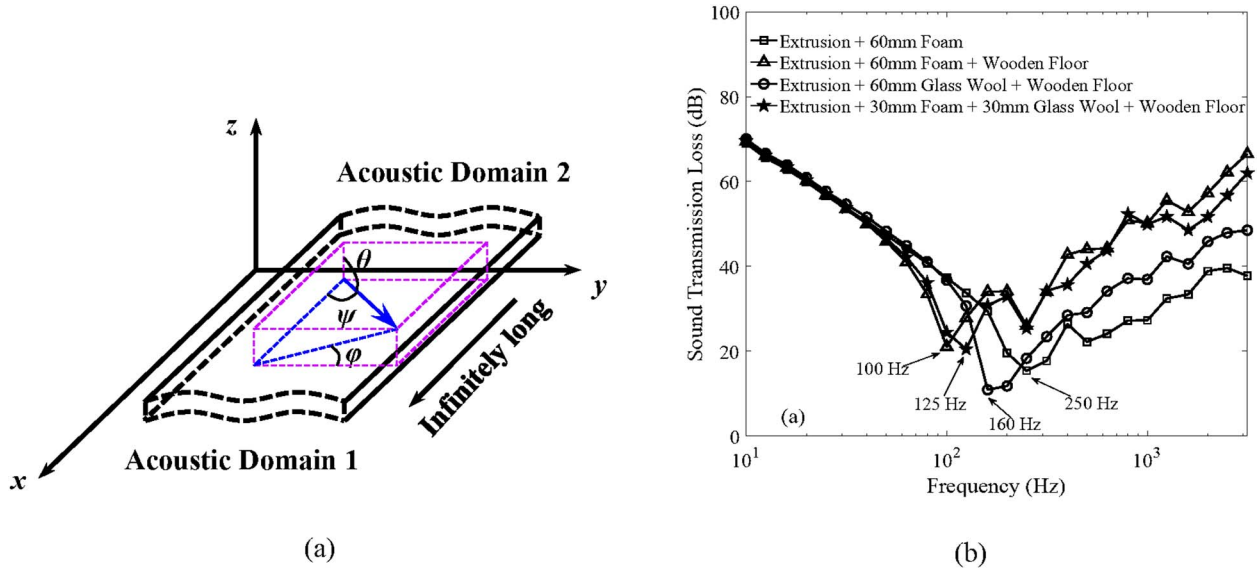

Figure 18. Influence of porous layer configuration on the diffuse field STL of the extrusion without the presence of the wooden beam. (a) Incident angles; (b) influence of porous layer configuration.

difficulties in doing so. One is that measured vibration data may be not sufficient due to the large number of forces to be determined. For example, for the bogie frame shown in Fig. 19, the number of forces applied to the frame is seventy-two. The other is that matrices to be inversed in the force identification process are ill-conditioned due to various reasons, such as structure resonances and measurement noise. Wang et al. (2022), Wang and Sheng (2022), and Wang (2023) present some efforts to overcome these difficulties. First, a time-domain response reconstruction method based on empirical wavelet transform is applied so that, although measurement is performed for a limited number of locations, responses of the bogie frame at other locations can be reconstructed, giving sufficient response data for force identification. If power is concerned, as in statistical energy analysis (SEA) (see Section 9), the responses of the structure at the loading points must be known. These responses may have to be reconstructed since direct measurement at these points is normally difficult. Second, with the measured and reconstructed responses, forces are identified using regularisation techniques developed for inverse problems. The methodology developed in Wang et al. (2022) Wang and Sheng (2022), and Wang (2023) is shown in Fig. 19, with application to a bogie frame. It requires vibration measurement and modal analysis of the bogie frame, as described below.

8.1. Vibration measurement on the bogie frame and modal analysis

The bogie frame is from the bogie under the driver's cabin. The bogie is shown in Fig. 20a and is a non-powered bogie. Ideally, there are measurement points which are as close to the loading points as possible and at the same time, no measurement point is located at a mode node of the structure. Limited by the measurement environment, only ten vibration acceleration sensors with twenty-four channels were arranged on the bogie frame, while the number of forces applied to the bogie frame is seventy-two. The layout of the measurement points on the bogie frame is depicted in Fig. 20b with the measured points indicated by symbol '⊗'. Measurement points 1B1, 1B2, 1B3, and 1B4 are just above the axle-box spring seat, 1B5 and 1B6 are near the air spring seats, 1B7 and 1B8 are above the traction rod seat, 1B9 and 1B10 are above the antiroll torsion bar seats.

The technique of response reconstruction developed in Wang and Sheng (2022) requires a modal analysis of the bogie frame. The analysis was performed based on a finite element model which was created from the 3D drawing of the frame provided by the manufacturer. The FE model is shown in Fig. 20b. Based on the *in situ* measured responses of the frame at the points shown in Fig. 20b, an operational modal analysis was performed to validate the FE model.

8.2. The nature of excitation

As a train runs along a track, wheel/rail vibrations are generated due to excitations from wheel/rail irregularities. The excitation is in general stochastic, but can be imposed with a periodic component at a single frequency, periodic impacts, or a combination of them. The excitation nature must be known when use is made of the technique of response reconstruction developed in Wang and Sheng (2022). The excitation nature may be determined from the measured vibration. Vibration data were sampled at a sampling frequency of 5,000 Hz, which is sufficiently high, given that train interior noise typically involves frequencies ranging from 20 to 800 Hz. Figure 21 shows the Fourier and envelope spectra of the vertical vibration accelerations measured at an axle box, the bogie frame, and the car body just above the bogie with the train running at 121, 156, 221, and 323 km/h. It can be seen that the Fourier spectra have modulation characteristics. The envelope spectra show that the fundamental characteristic frequencies are, respectively, 11.60, 14.34, 21.97, and 31.13 Hz, equal to the corresponding rotation frequencies of the wheel, which has a diameter of 920 mm. This indicates that one of the wheels creates periodically impulsive excitations to the bogie.

8.3. Forces applied to the bogie frame

With the measured and reconstructed responses of the bogie frame, forces applied to the bogie frame by the suspensions can be determined in the time domain. Use is made of the time-domain

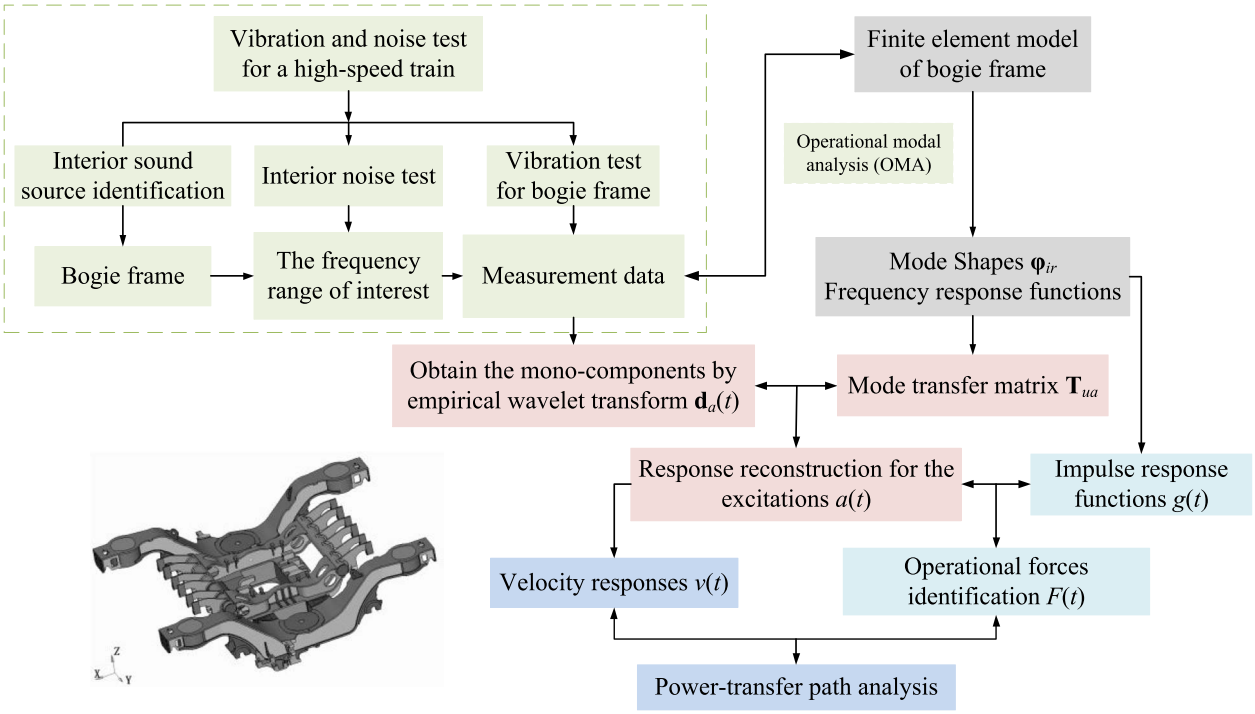

Figure 19. A flowchart of load identification for a high-speed train bogie frame under operational conditions based on the time-domain response reconstruction.

Figure 20. The bogie, bogie frame, and measurement points. (a) A photo of the bogie; (b) the layout of measurement points on the bogie frame.

impulse response function of the bogie frame which is calculated based on the FE model. For a linear time-invariant system subject to a force vector $\mathbf{f}(t)$, the system response can be expressed as the following convolution integral

$$\mathbf{y}(t) = \mathbf{H}(t) * \mathbf{f}(t) = \mathbf{y}(0) + \int_0^t \mathbf{H}(t-\tau)\,\mathbf{f}(\tau)\,d\tau \tag{2}$$

where $\mathbf{y}(t)$ is the response, $\mathbf{H}(t)$ is the associated impulse response function matrix of the system and is of order $M \times N$ with M being the number of known responses and N being that of the unknown forces. The convolution integral in Equation (2) can be discretised into a matrix form

$$\begin{Bmatrix} \mathbf{y}(t_1) - \mathbf{y}(0) \\ \mathbf{y}(t_2) - \mathbf{y}(0) \\ \cdots \\ \mathbf{y}(t_J) - \mathbf{y}(0) \end{Bmatrix} = \mathbf{G} \begin{Bmatrix} \mathbf{f}(t_0) \\ \mathbf{f}(t_1) \\ \cdots \\ \mathbf{f}(t_{J-1}) \end{Bmatrix} \tag{3}$$

where $t_j = (j-1)\,\Delta t, j = 1, 2, \cdots J$, and $\mathbf{G}$ is a matrix of order $MJ \times NJ$. In order to ensure a unique solution for the equation, it is usually required that the number of measurement points (or dofs) should be greater than that of the external excitations, typically by a factor 2 as a rule of thumb.

Due to inevitable noise and error in the responses and the ill-conditioned characteristic of matrix $\mathbf{G}$, force identification, as an inverse problem, is usually ill-posed and difficult to find an accurate solution by using the least-square method. Alternative methods should be applied. In Wang et al. (2022), to reduce any inversion instability, different regularisation processes, including Tikhonov regularisation, truncated singular value decomposition and L1-regularised least squares (L1_ls), are employed and compared.

With the identified forces and the reconstructed responses at the loading points, powers flowing to (positive), or out of (negative), the bogie frame are predicted in Wang (2023) and shown in Fig. 22. The results are based on vibration data measured on the bogie frame when the train was running along the embankment section (see Section 2). It can be seen that elements in the primary suspension supply powers to the bogie frame with the vertical damper and the steel spring being the main contributors. Part of the power received by the bogie frame is dissipated by damping

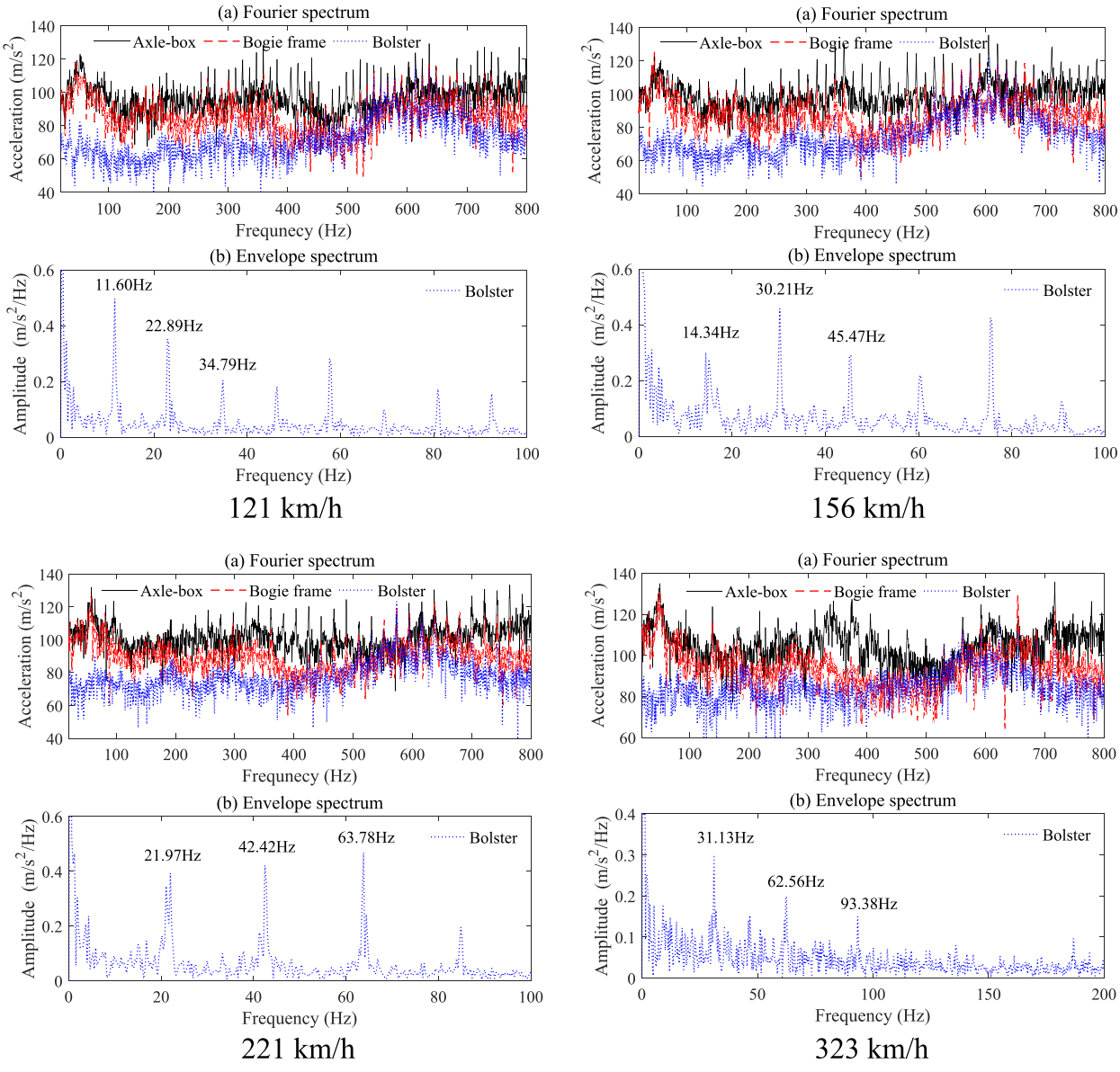

Figure 21. The spectrum of the measured vibration acceleration.

in the bogie frame and the remaining part flows to the secondary suspension, mainly through the vertical damper and the antiroll torsional bar.

9. SEA-based prediction of train interior noise

Train companies are increasingly interested in predicting train interior noise because an accurate and efficient prediction model can serve as a design tool in the development of new trains. It seems to be a fact that prediction of train interior noise is extremely difficult, especially for high-speed trains using 'accurate methods' such as the finite element method and boundary element method, due to the wide frequency range (up to about 1,000 Hz), the composited structure of the car body, and the complicated nature of the noise sources. This gives opportunities for the 'less accurate' methods, such as the SEA method, to play a role in the prediction of train interior noise.

SEA provides a simple, intuitive model of the vibration/acoustics of a structure which is based on the flow and distribution of vibrational/acoustical energy through the structure. The structure is divided into a set of subsystems and each subsystem is described by a few gross properties (e.g. size, mass) and no details; It predicts average noise and vibration levels: time (over the period of each harmonic vibration) and frequency (normally over each 1/3 octave band) averages, together with average over positions within each subsystem; It gives a coarse idealisation of the behaviour of the structure, without the detail of the response (i.e. not the response at a point at a specific frequency). This is justified by that such detail may be illusory, because of the effects of uncertainty and variability.

The SEA equations involve various approximations and assumptions: (1) richness of modes: each subsystem has at least three modes in each frequency band concerned; the modes are alternatively termed oscillators; (2) uncorrelated modal forces: modal forces associated with each oscillator are uncorrelated; (3) equipartition of modal energy: the energies

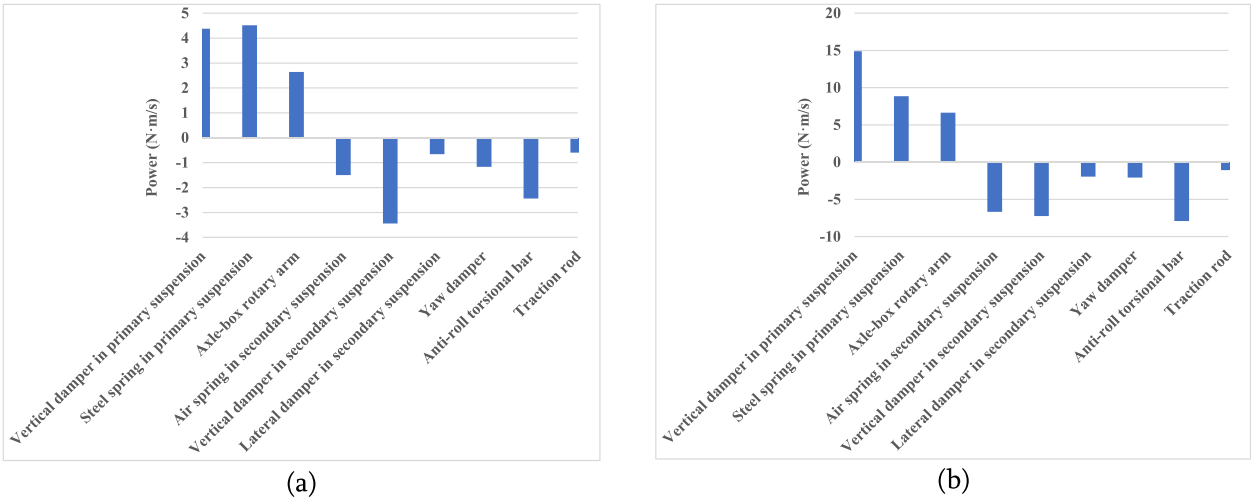

Figure 22. The overall powers (0–800 Hz) flowing to, or out of, the bogie frame. (a) at 250 km/h; (b) at 350 km/h.

of the modes are roughly the same; (4) weak coupling: the interaction of two oscillators is not affected by the presence of a third oscillator, nor of the presence of a third subsystem; direct modal coupling within each subsystem is negligible; modal coupling within a subsystem via the other subsystem is negligible; (5) coupling power proportionality: the energy flow between two conservatively coupled linear subsystems excited by broadband forces is proportional to the difference in the average modal energies.

Although these approximations and assumptions cannot be fully satisfied when applying SEA to predict train interior noise, SEA model is increasingly demonstrated to be useful to predict interior noise for a typical high-speed train, especially when the model is used to predict the effect of design change after the SEA model has been updated with measurement. One of the applications is presented in Zhang et al. (2016) for the dining coach in a high-speed train. Figure 23 displays a set of views of the SEA model, which consists of several plate subsystems and acoustic cavity subsystems. The subsystems of the coach are created in such a way that, on the one hand, they reflect the structural features of the coach, and on the other hand, each subsystem includes as many modes as possible. In total, the SEA model consists of approximately 500 subsystems, including 50 floor subsystems, 160 sidewall subsystems, 70 roof subsystems, 100 interior cavity subsystems, 70 exterior cavity subsystems, and other subsystems. Diffuse acoustic fields (DAFs) and constraints are applied on the exterior acoustic cavity subsystems into which noise source powers are injected. Sources include bogie area noise, aerodynamic noise, and equipment area noise. Semi-infinite fluids are created and connected to the exterior acoustic cavity subsystems to simulate the outside acoustic environment. Additionally, vibrations measured on the floor, sidewall, roof, and dining coach panel divider are specified for plate subsystems as constraints. Doing so means to assume that the vibrations specified can largely represent structure-borne vibration, so that only noise sources need to be considered in the SEA model. However, the measured vibration contains not only the part excited by vibration transmission, but also the other part excited by noise. It is still unclear which one is more important for a given frequency band.

A SEA model requires input power, modal density, internal loss factor, and coupling loss factor for each subsystem. In Zhang et al. (2016), all parameters are determined experimentally, and the comparison between the predicted and measured interior noise is shown in Fig. 24. The comparison is so promising that an acoustic design procedure for controlling interior noise of high-speed trains is proposed in Zhang et al. (2020b).

The accuracy of the SEA-based interior noise prediction model largely depends on the SEA parameters. Different methods to obtain those parameters are improved and proposed. Internal loss factor is normally determined experimentally and modal density can be determined either analytically (numerically) or experimentally. In Zhang et al. (2020c), the double-exponential windowing method developed in Sheng (2012) is improved to identify modal frequencies and damping ratios (internal loss factors) of dynamically large structures (like the floor, sidewall and roof subsystems in Zhang et al. [2016]). Since many structure subsystems are uniform in the longitudinal direction, the modal density of such a subsystem can be estimated based on the group speeds of the otherwise infinite long structure, while the group speeds can be calculated based on the 2.5D finite element method, as shown in Zhang et al. (2022). The coupling loss factor between a panel subsystem and an air cavity may be determined experimentally using two reverberation rooms. The coupling loss factor between two composite panel subsystems may be determined following the idea of experimental SEA applied to these two subsystems.

10. Concluding remarks

This paper is not a comprehensive literature review, but only summaries researches carried out in recent years by the authors and their teams into high-speed railway noise. It presents measurement results showing typical characteristics of high-speed railway noise, an analyse on source contribution to pass-by noise based on microphone array measured data, modelling of high-speed rolling noise, aerodynamic noise and viaduct bridge noise, prediction and control of the vibro-acoustic behaviour of car-body with poro-elastic media, an analyse of vibration transmission in the suspension/bogie system, and SEA-based prediction of train interior noise. The paper is mainly focused on methods developed for predicting and analysing high-speed railway noise, e.g. the

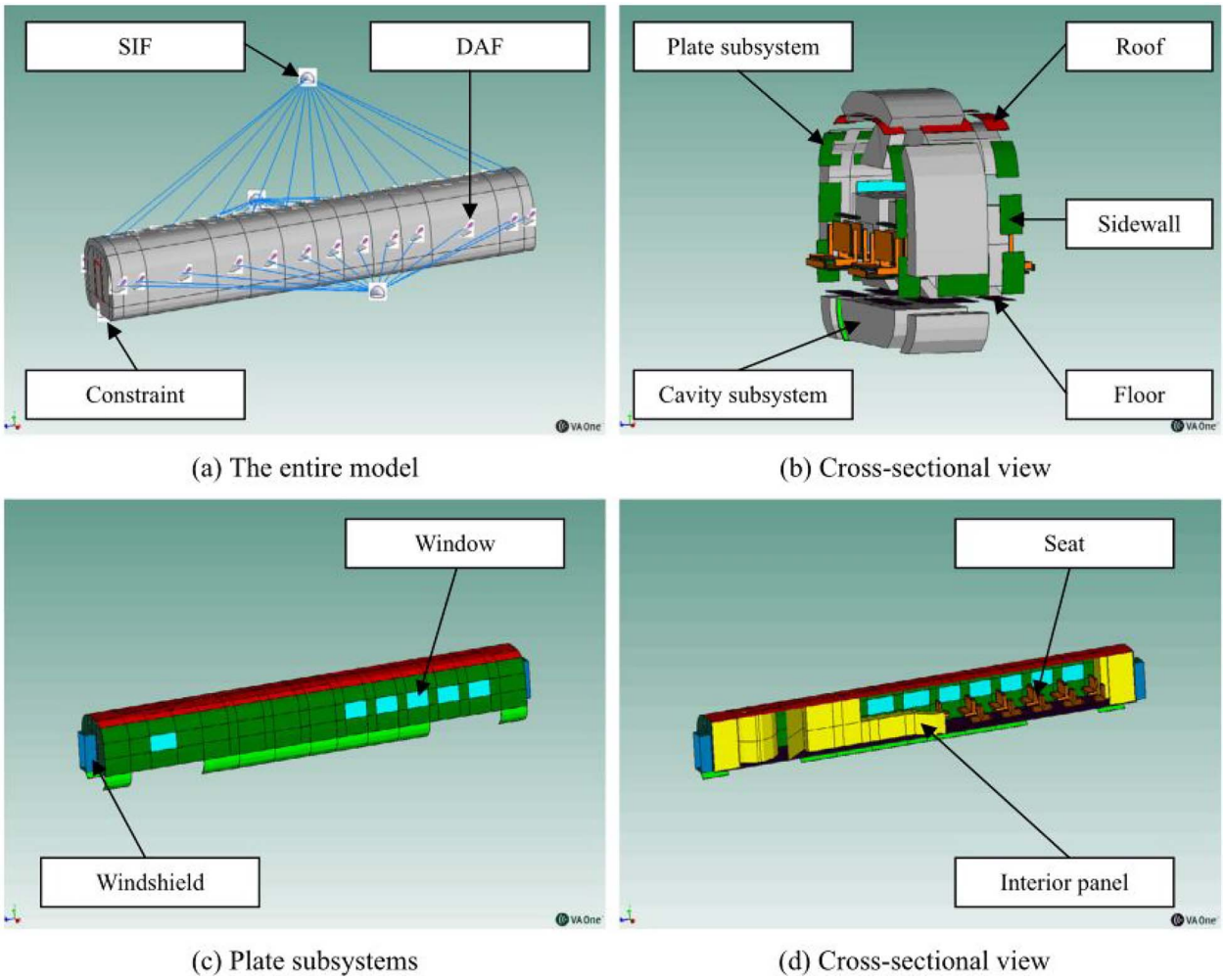

Figure 23. Different views of the SEA model.

method for quantifying and ranking noise sources on a moving train based on microphone array measurement and the pass-by noise prediction model; the method for predicting wheelset dynamics considering all the effects of rotation; the method for predicting track dynamics using a periodic structure approach; the method for predicting sound radiation from a moving wheel based on sound spectra generated by moving harmonic compact sources; the method for estimating forces transmitted by a bogie based purely on vibration measurement; etc.

Due to the much more complicated nature of train interior noise and some other reasons, the paper has presented results mainly for train pass-by noise, rather than train interior noise. In terms of pass-by noise at the specified measurement points, the main contributor is the bogie areas which emit noise both vibro-acoustically and aerodynamically. It is concluded that, for the track and train studied, the overall pass-by noise level in dB(A) is dominated by rolling noise, even at 350 km/h. It is predicted that the rail contributes more than the wheels, although this has not been verified by *in situ* measurement. It is expected that in the development of 400 km/h high-speed trains, controlling rolling noise is at least as important as controlling aerodynamic noise. To control rolling noise, measures may have to be applied to both the wheel and rail.

Some open problems on high-speed railway noise are also discussed, and they can be topics of further research. The importance of the topics may be enhanced by the development of trains running at higher speeds. The open problems discussed in this paper are summarised as below:

(1) How to separate contributions to pass-by noise between the aerodynamic noise of the moving bogie, the rolling noise of the wheel, and rolling noise of the rail based on microphone array measurement?
(2) There is strongly nonuniform airflow around the train and what is the effect of such flow on wheel/rail rolling noise generation and propagation?
(3) How important are the periodic gaps formed by the rail, fasteners, and slab to rolling noise generation?
(4) Aerodynamic noise from a moving wheel is predicted by assuming the wheel to be a rigid body, while vibro-acoustic noise from the moving and vibrating wheel is predicted by assuming still air around the wheel. What is the effect of these assumptions? Especially for trains running at 400 km/h?
(5) How to improve aeroacoustic scaling laws for aerodynamic noise from high-speed trains running at higher speeds (e.g. 400 km/h and above) so that results from downscaled models are more useful?
(6) At 400 km/h or higher, how important is air compressibility to aerodynamic noise generation?

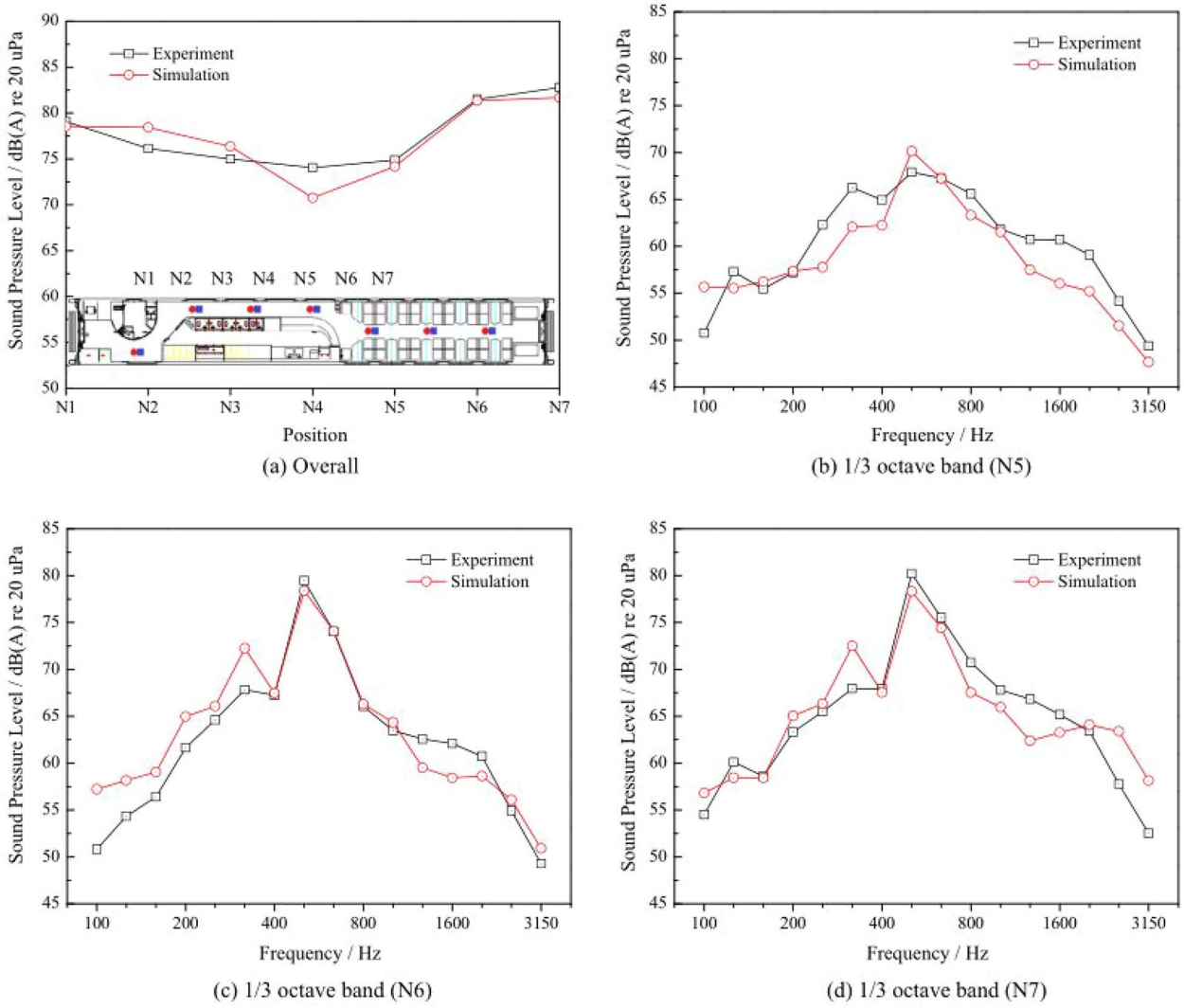

Figure 24. Comparison between prediction and experimental results.

(7) In addition to the air-borne and structure-borne noise, is the turbulent boundary layer of the train body a significant source to interior noise at 400 km/h?

Acknowledgements

Most of the results reported in this paper are parts of the outcomes of the following projects:

(1) Project (52272352, 2023-2026) founded by the National Natural Science Foundation of China: Research on the vibro-acoustic characteristics of a cyclically periodic wheelset rotating and moving at high speed;
(2) Project (U1934203, 2020-2023) founded jointly by the National Natural Science Foundation of China and China Railway: Research on combined vibration and acoustic comfort of high-speed train;
(3) Project (U1834201, 2019-2022) founded jointly by the National Natural Science Foundation of China and China Railway: Generation, propagation and control of high-speed railway noise;
(4) Project (2016YFE0205200, 2017-2021) founded by the Ministry of Science and Technology of the People's Republic of China as part of the National Key Research and Development Program: Joint research into key technologies for controlling noise and vibration of high-speed railways under extremely complicated conditions;
(5) Project (2015Z003-B, 2015-2017) founded by China Railway: High-speed railway noise control technologies—generation mechanisms, transfer paths and key parameters of high-speed train interior noise;
(6) Project (U1434201, 2015-2018) founded jointly by the National Natural Science Foundation of China and China Railway: Theory and method of vibration and noise reduction of high-speed train wheel and rail.

Author contributions

Xiaozhen Sheng: Writing all sections apart from 5 and 9; Reviewing and editing; Shumin Zhang: Writing Section 9; Xinbiao Xiao: Discussion and data re-processing; Yuan He: write Section 5.

Supplementary data

Supplementary data are available at *ITINFR Journal* online.

Conflict of Interest statement

One of the authors, Dr. Xiaozhen Sheng, is an associate editor of Intelligent Transportation Infrastructure. He was blinded from reviewing or making decisions on the manuscript.

References

Biot, M. A. (1956a) 'The Theory of Propagation of Elastic Waves in a Fluid-Saturated Porous Solid. I. Low-Frequency Range', *Journal of the Acoustical Society of America*, **28**: 168–78.

Biot, M. A. (1956b) 'Theory of Propagation of Elastic Waves in a Fluid-Saturated Porous Media. II. Higher-Frequency Range', *Journal of the Acoustical Society of America*, **28**: 179–91.

Cheng, G. *et al.* (2021) 'An Investigation into the Effects of Modelling Assumptions on Sound Power Radiated from a High-Speed Train Wheelset', *Journal of Sound and Vibration*, **495**: 115910.

Deng, T. *et al.* (2021) 'A Two-and-Half Dimensional Finite Element/Boundary Element Model for Predicting the Vibro-Acoustic Behaviour of Panels with Poro-Elastic Media', *Journal of Sound and Vibration*, **505**: 116147.

He, B. *et al.* (2014) 'Investigation into External Noise of a High-Speed Train at Different Speeds', *Journal of Zhejiang University (Applied Physics & Engineering)*, **15**: 1019–33.

He, Y. (2023) *Aerodynamic Noise Simulation of High-Speed Train Bogie*. PhD thesis, Southampton University, Southampton, UK.

He, Y. *et al.* (2021) 'Modelling Noise Radiation from Concrete Box Girder Bridges as an Infinitely Long Periodic Structure Excited by a High-Speed Train', *Journal of Vibration and Acoustics*, **143**: 031015.

Latorre Iglesias, E. *et al.* (2017) 'Anechoic Wind Tunnel Tests on High-Speed Train Bogie Aerodynamic Noise', *International Journal of Rail Transportation*, **5**: 87–109.

Lauterbach, A. *et al.* (2012) 'Microphone Array Wind Tunnel Measurements of Reynolds Number Effects in High-Speed Train Aeroacoustics', *International Journal of Aeroacoustics*, **11**: 411–46.

Li, M. *et al.* (2021a) 'Analysis of Source Contribution to Pass-by Noise for a Moving High-Speed Train Based on Microphone Array Measurement', *Measurement*, **174**: 109058.

Li, M. *et al.* (2021b) 'An Investigation into High-Speed Train Interior Noise with Operational Transfer Path Analysis Method', *Railway Engineering Science*, **29**: 1–14.

Li, Q., Li, Z. and Yang, Z. (2022) 'Noise Contribution and Coherence Analysis of High-Speed Train Head Shape under Moving Slab Track', *Proceedings the Institution of Mechanical Engineers, Part F: Journal of Rail and Rapid Transit*, **237**: 848–57.

Li, Q., Song, X. and Wu, D. (2014) 'A 2.5-Dimensional Method for the Prediction of Structure-Borne Low-Frequency Noise from Concrete Rail Transit Bridges', *The Journal of the Acoustical Society of America*, **135**: 2718–26.

Li, X., Liang, L. and Wang, D. (2018) 'Vibration and Noise Characteristics of an Elevated Box Girder Paved with Different Track Structures', *Journal of Sound and Vibration*, **425**: 21–40.

Mellet, C. *et al.* (2006) 'High-Speed Train Noise Emission: Latest Investigation of the Aerodynamic/Rolling Noise Contribution', *Journal of Sound and Vibration*, **293**: 535–46.

Noh, H. M. (2017) 'Contribution Analysis of Interior Noise and Floor Vibration in High-Speed Trains by Operational Transfer Path Analysis', *Advances in Mechanical Engineering*, **9**: 1–14.

Sheng, X. (2012) 'A New Experimental Modal Analysis Method Based on Double-Exponential Windowing and Application to Lightly Damped Bladed Wheels', *Journal of Sound and Vibration*, **331**: 2824–35.

Sheng, X. (2015) 'Generalization of the Fourier Transform-Based Method for Calculating the Response of a Periodic Railway Track Subject to a Moving Harmonic Load', *Journal of Modern Transportation*, **23**: 12–29.

Sheng, X., Cheng, G., and He, Y. 'Dynamics of a Train Wheelset in Rotation', https://www.researchgate.net/publication/361182130_Dynamics_of_a_train_wheelset_in_rotation.

Sheng, X., Cheng, G. and Thompson, D. J. (2020) 'Modelling Wheel/Rail Rolling Noise for a High-Speed Train Running Along an Infinitely Long Periodic Slab Track', *Journal of the Acoustical Society of America*, **148**: 174–90.

Sheng, X., Jones, C. J. C. and Thompson, D. J. (2005) 'Responses of Infinite Periodic Structures to Moving or Stationary Harmonic Loads', *Journal of Sound and Vibration*, **282**: 125–49.

Sheng, X. *et al.* (2007) 'Using the Fourier-Series Approach to Study Interactions between Moving Wheels and a Periodically Supported Rail', *Journal of Sound and Vibration*, **303**: 873–94.

Sheng, X., Peng, Y. and Xiao, X. (2019) 'Boundary Integral Equations for Sound Radiation from a Harmonically Vibrating Body Moving Uniformly in a Free Space', *Journal of the Acoustical Society of America*, **146**: 4493–506.

Sheng, X., Xiao, X. and Zhang, S. (2016) 'The Time-Domain Moving Green Function of a Railway Track and its Application to Wheel–Rail Interactions', *Journal of Sound and Vibration*, **377**: 133–54.

Sheng, X., Zhong, T. and Li, Y. (2017) 'Vibration and Sound Radiation of Slab High-Speed Railway Tracks Subject to a Moving Harmonic Load', *Journal of Sound and Vibration*, **395**: 160–86.

Shi, J. (2020) Prediction and Control of Aerodynamic Noise of High-Speed Pantograph in Low Temperature Environment. MSc Thesis, Southwest Jiaotong University, Chengdu, China.

Ström, R. (2014) Operational Transfer Path Analysis of Components of a High-Speed Train Bogie. PhD thesis, Chalmers University of Technology, Göteborg, Sweden.

Theyssen, J. *et al.* (2023) 'On the Efficient Simulation of Pass-by Noise Signals from Railway Wheels', *Journal of Sound and Vibration*, **564**: 117889.

Thompson, D. J. (2009) *Railway Noise and Vibration: Mechanisms, Modelling and Means*. London, UK: Elsevier.

Thompson, D. J., Fodiman, P. and Mahe, H. (1996b) 'Experimental Validation of the TWINS Prediction Program for Rolling Noise, Part 2: Results', *Journal of Sound and Vibration*, **193**: 137–47.

Thompson, D. J., Hemsworth, B. and Vincent, N. (1996a) 'Experimental Validation of the TWINS Prediction Program for Rolling Noise, Part 1: Description of the Model and Method', *Journal of Sound and Vibration*, **193**: 123–35.

Thompson, D. J. *et al.* (2015) 'Recent Developments in the Prediction and Control of Aerodynamic Noise from High-Speed Trains', *International Journal of Rail Transportation*, **3**: 119–50.

Wang, M. (2023) Analysis of Vibration Transmission Characteristic for the Bogie System of a High-Speed Train under Operational Conditions. PhD thesis, Southwest Jiaotong University, Chengdu, China.

Wang, M., and Sheng, X. (2022) 'Combining Empirical Wavelet Transform and Transfer Matrix or Modal Superposition to Reconstruct Responses of Structures Subject to Typical Excitations', *Mechanical Systems and Signal Processing*, **163**: 108162.

Wang, M. *et al.* (2022) 'Estimation of Vibration Powers Flowing to and out of a High-Speed Train Bogie Frame Assisted by Time-Domain Response Reconstruction', *Applied Acoustics*, **185**: 108390.

Yang, Y. *et al.* (2019) 'Analysis on Exterior Noise Characteristics of High-Speed Trains in Bridges and Embankments Section Based on Experiment', *Chinese Journal of Mechanical Engineering*, **55**: 188–97 (In Chinese).

Zhang, J. *et al.* (2020b) 'An Acoustic Design Procedure for Controlling Interior Noise of High-Speed Trains', *Applied Acoustics*, **168**: 107419.

Zhang, J. *et al.* (2016) 'SEA and Contribution Analysis for Interior Noise of a High-Speed Train', *Applied Acoustics*, **112**: 158–70.

Zhang, S. *et al.* (2020a) 'Dynamic Wheel-Rail Interaction at High Speed Based on Time-Domain Moving Green's Functions', *Journal of Sound and Vibration*, **488**: 115632.

Zhang, S., Sheng, X. and Yang, S. (2022) 'Modal Density Calculation of Finite Length Waveguide Structure Based on 2.5D Finite Element Method', *Journal of Vibration and Shock*, **41**: 90–8 (In Chinese).

Zhang, S. *et al.* (2020c) 'Improving the Double-Exponential Windowing Method to Identify Modal Frequencies and Damping Ratios of Dynamically Large Structures', *Journal of Sound and Vibration*, **476**: 115314.

Zhang, X. *et al.* (2013) 'Theoretical and Experimental Investigation on Bridge-Borne Noise under Moving High-Speed Vehicle', *Science China Technological Sciences*, **56**: 917–24.

Zhang, Y. *et al.* (2018) 'Sound Transmission Loss Properties of Truss Core Extruded Panels', *Applied Acoustics*, **131**: 134–53.

Zhao, Y. *et al.* (2020) 'Analysis of the Near-Field and Far-Field Sound Pressure Generated by High-Speed Trains Pantograph System', *Applied Acoustics*, **169**: 107506.

Zhong, T. *et al.* (2018) 'Vibration and Sound Radiation of a Rotating Train Wheel Subject to a Vertical Harmonic Wheel–Rail Force', *Journal of Modern Transportation*, **3**: 1–15.

Zhu, J., Hu, Z. and Thompson, D. J. (2017) 'The Effect of a Moving Ground on the Flow and Aerodynamic Noise Behaviour of a Simplified High-Speed Train Bogie', *International Journal of Rail Transportation*, **5**: 110–25.